Stockholm University

Bachelor Thesis

Degree Project
in Marine Geology 30 hp

Bottom habitat mapping east of Askö Island south of the Stockholm Archipelago

Valerie Pernius

Stockholm 2023

Department of Geological Sciences
Stockholm University
SE-106 91 Stockholm
Sweden

Abstract

The field of marine surveying and mapping has rapidly expanded in recent decades due to continuous advancements in instrument technology and growing applications of acquired data. Multibeam echo sounders (MBES) have dominated this field owing to the versatility and high resolution of the data obtained by this system. This project focused on utilizing backscatter data from multibeam surveys conducted east of Askö Island to categorize seafloor sediments. Maps representing seafloor sediment composition and seabed characteristics were created to provide information about bottom habitats in the study area. Seafloor habitat maps are vital resources for benthic ecosystem conservation, marine resource management, and the continued study of submarine geomorphological processes. However, there is currently no standardized approach to seafloor classification and habitat mapping based on backscatter data. This project employed semi-automatic data processing software as the primary tool for interpreting backscatter and generating sediment classifications. Habitat maps of Askö Island's eastern seafloor were produced, reflecting the characterizations made through data processing. To verify the accuracy of software-generated products, sediment core samples collected from the study area were used for comparative analysis. The findings in this study demonstrate that only general interpretations are achievable based on backscatter data alone. Nevertheless, existing technologies can be adapted to produce valuable products from the remotely surveyed seafloor data.

Key terms: acoustic backscatter, multibeam echo sounder, sediment classification, habitat mapping, Angle vs. Range Analysis

For Cornelia, my perpetual source of motivation.

Acknowledgements

I would like to express my great gratitude to my supervisor, Prof. Martin Jakobsson, who first introduced me to the field of marine geophysics. What began as an introduction has quickly evolved into one of my deepest passions.

I would also like to extend my heartfelt appreciation to Prof. Alasdair Skelton, whose constant support and encouragement helped solidify my love for geology.

To Prof. Jakobsson and Prof. Skelton, thank you for sharing your expertise and for the numerous opportunities you have provided me to explore my interests. I feel fortunate to have had such exceptional mentors.

TABLE OF CONTENTS

1. INTRODUCTION

Since its first research applications in the late 20th century, the field of seafloor mapping with echo sounders has rapidly expanded with continuous advancements in instrumentation technology, post-processing algorithms, and new potential applications for obtained geophysical data (Kenny et al., 2003). Multibeam echo sounder (MBES) systems have dominated this field owing to their ability to provide high-resolution imagery while covering a wide swath of the seafloor (Brown et al., 2011). While MBES are primarily utilized to resolve ocean bathymetry, the echo-strength measurement returned from the esonified seafloor, also known as *backscatter*, is simultaneously logged by several systems, and can be further processed to provide insights into the composition of the seafloor (Parnum and Gavrilov, 2011). The substrate types, grain sizes, and possible benthic habitat conditions can potentially be inferred. Acoustic measurements are commonly combined with in-situ sampling or *ground truths* to generate accurate seafloor bottom habitat maps of a region (Parnum and Gavrilov, 2011). However, relying on backscatter data for sediment classification and sequential habitat mapping is theoretically possible. The aim of this project is to explore this possibility by utilizing backscatter data from multibeam geophysical surveys east of Askö Island to create a benthic habitat map of the region. A select set of in-situ data are used in this project to enable comparative analysis between the generated and observed seafloor classifications.

Benthic habitats can be defined as "spatially defined areas where the physical, chemical and biological environment is distinctly different from the surrounding" seafloor (Kostylev et al., 2011). While this definition varies between scientific disciplines, the field of geophysical mapping generally relies on surface sediments and seafloor morphology to define habitat boundaries (Brown et al., 2011). The successful creation of benthic habitat maps depends largely on the ability to convert geophysical data related to the bottom substrate into significant indicators of the benthic habitats (Diaz et al., 2004).

Seafloor sediments are rarely defined by linear boundaries. To identify and categorize gradual margins between seabed sediments and features, the incorporation of in-situ investigations is generally encouraged to complement remotely obtained data (Brown et al., 2011). A combination of biological and geophysical investigations can be used for this purpose. Accurate classification of the seafloor can potentially play a vital role in ecosystem conservation efforts, as well as in the effective management of marine resources and coastal environments (Craig et al., 2011). Furthermore, these classifications can contribute to our understanding of underwater geomorphological processes and sedimentation regimes.

Currently, there is no standardized approach to classifying backscatter data for the purpose of benthic habitat mapping (Diaz et al., 2004). Numerous habitat classification methods have been explored in recent decades, primarily relying on seafloor morphology for delineating habitat classes (Smith et al., 2015). Still, a definitive standard has not been formally adopted yet. Researchers have developed algorithms that offer automated postprocessing interpretations of the seafloor based entirely on acoustic backscatter properties (White et al., 2007). However, these interpretations are generally regarded as guidelines, and may not always be acknowledged as precise seafloor classification methods. Given the significant variation among marine geophysical mapping methods, surveyors and data processors must ultimately determine the most appropriate methods for individual surveys and purposes.

Multibeam echo sounder (MBES) systems are ordinarily used to collect data relevant to seafloor habitat classifications. MBES surveys use the basic principle of echo-sounding to determine a region’s bathymetry. The depth of the surveyed seafloor can be established by calculating the two-way travel time (TWT), defined as the time taken for a transmitted acoustic pulse to reach the seafloor and return to the system receiver (Jakobsson et al., 2016). However, the dynamic nature of seawater composition, temperature, and pressure require the calculation of sound velocity profiles (SVP) to convert time-travel measurements into accurate distances (White et al., 2007). Meanwhile, backscatter data rely on the measured intensity of returning acoustic signals (dB) to interpret the surface characteristics of the seafloor (Parnum and Gavrilov, 2011). This data is commonly visualized in the form of grayscale, georeferenced mosaics representing brighter and darker areas with stronger and weaker acoustic returns, respectively (Che Hasan et al., 2014). Backscatter data is simultaneously logged during most MBES surveys, although systems are seldom calibrated with focus on backscatter data acquisition (Fonseca and Mayer, 2007). Although there is no standardized technique for processing backscatter data, geometric and radiometric corrections can be applied to create reliable sediment interpretations (Fonseca and Mayer, 2007). One such approach is Fonseca and Calder’s (2015) method of removing backscatter angular response variations to generate homogenous swaths of the surveyed seafloor (Fonseca et al., 2009). By removing backscatter strength variations caused by radiometric errors, it is hypothetically possible to retrieve backscatter data representative of seafloor properties. Fonseca and Calder’s (2015) processing method was employed in this project, using their Geocoder Toolbox algorithm to process backscatter data.

Marine geophysical data collected during Stockholm University’s yearly course “Marine Geophysical Mapping Methods”, were used as the foundation for this study. The field work is confined to an area east of Askö Island, where permission to conduct seafloor mapping and openly distribute the data has been granted by the Swedish Armed Forces and Swedish Maritime Administration.

2. BACKGROUND

2.1 Survey Area

Askö Island (58° 49’ 21” N, 17° 38’ 55” E), south of the Stockholm archipelago serves as the focal point of this project (*Figure 1*). The study area covers the northeastern region of Askö and the surrounding seafloor bordering Boknö-Oxnö, Brännskär, Kråmo, Korpen, Oxnö and Fifång (*Figure 2*). The marine geophysical data used for this project was collected between 2012 - 2022 during Stockholm University’s yearly fieldwork in the course “Marine Geophysical Mapping Methods”, 7.5 hp, GG4071. An approximate area of 45 km² of seafloor was surveyed at depths ranging from 10 to 54 meters below sea-level.

OVERVIEW MAP

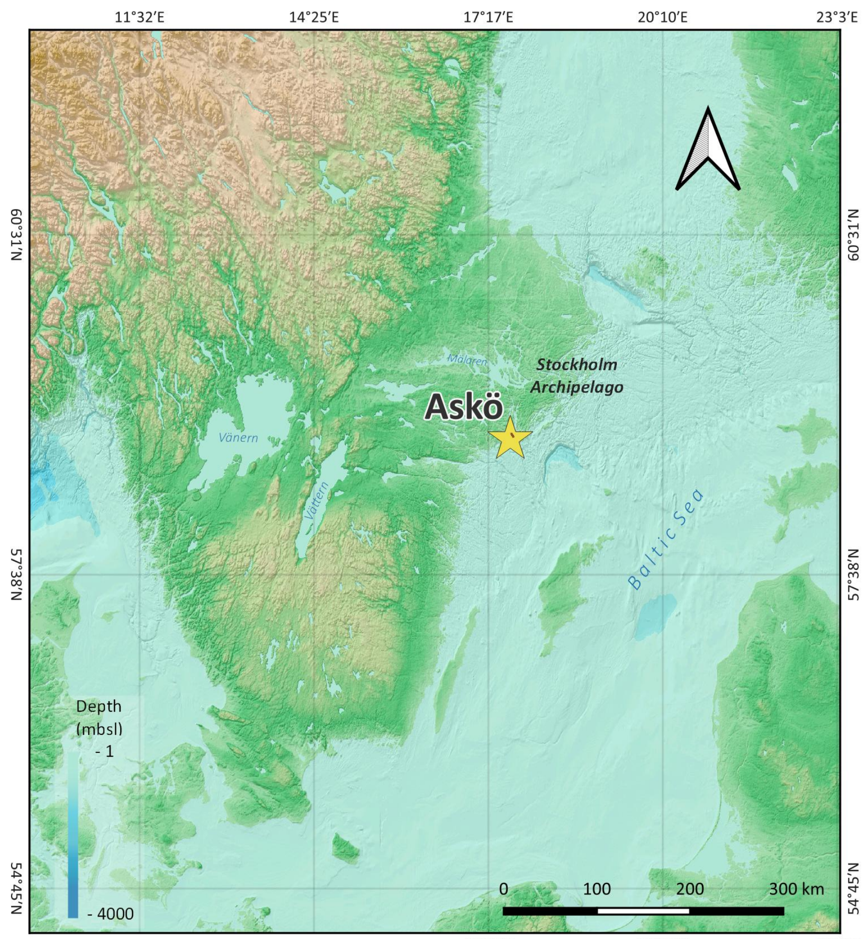

Figure 1. Overview map of central and southern Sweden, showing the location of Askö Island and the general locality of the Stockholm Archipelago. Askö is marked by a yellow star, approximately 60 km southwest of the central Stockholm Archipelago label. The Baltic Sea and major Swedish lakes are labeled in blue.
The bathymetry data, topography and seafloor features on this map were created by the GEBCO Compilation Group (2022) as global gridded bathymetric data sets. The color scale used for this grid displays shifts in the Baltic Sea depths at roughly - 200 meters. This illustration was created on QGIS using GEBCO’s online database, displayed as a Web Coverage Service (WCS) digital layer. CRS: ESPG:3857 - WGS 84 / Pseudo-Mercator.

STUDY AREA

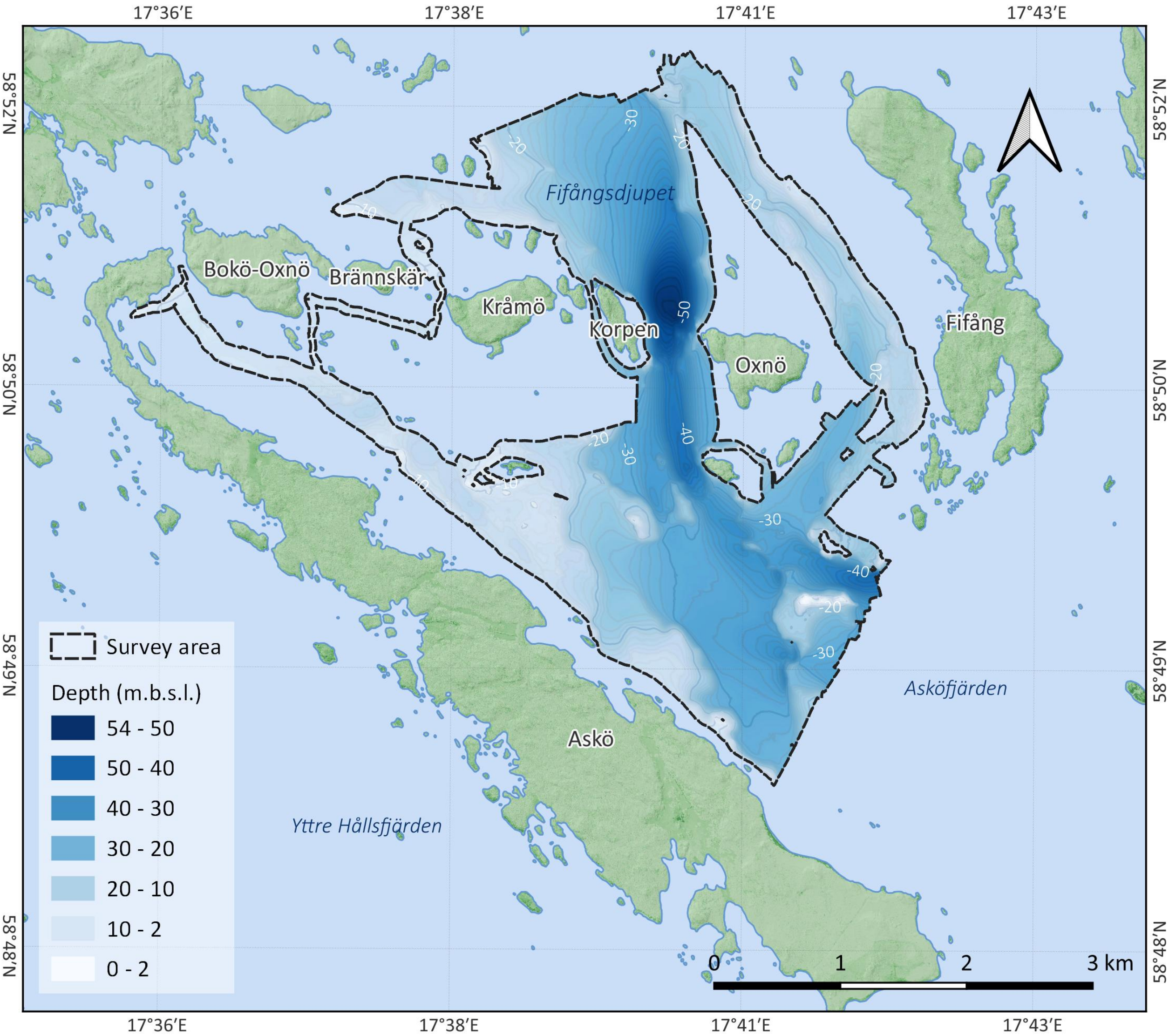

Figure 2. Map of the study area marked by a dashed outline, northeast of Askö Island. The surveyed seafloor area is surrounded by Bokö-Oxnö, Brännskär, Kråmo, Korpen, Oxnö and Fifång islands. Multibeam bathymetry data collected and processed by Jakobsson et al., (2020) on QPS Qimera, was used to create contours and shaded relief of the seafloor. White numbers within the survey area represent depth measurements at 10 m depth intervals, while contour lines are shown for every meter. The names of the local bays and deep are displayed in blue. The satellite imagery and digital map data used to create this map were provided by Lantmäteriet via the Swedish University of Agricultural Sciences (SLU) geodata portal. Visualizations are projected in Coordinate Reference System (CRS) SWEREF99 18 00, EPSG: 3011.

2.1.1 Askö Region and the Stockholm Archipelago

The official limit of the southern Stockholm Archipelago varies between publications, some including Askö within its boundary and others, not. In this study, Askö region is denoted a part Trosa Archipelago, immediately south of the Stockholm Archipelago as defined by Kautsky, (2008).

The Trosa Archipelago contains approximately 2,800 islands and several islets of various sizes. Askö area is considered an open archipelago, which spreads across an area of roughly 365 km^2. In contrast, the Stockholm Archipelago is composed of approximately 20,000 islands, stretching about 200 km along the east coast of Sweden. Most of the islands lie within the Northern Baltic Proper and continue south into the Western Gotland Basin (Jakobsson et al., 2019) (*Figure 3*). Traditionally, the Stockholm Archipelago has been divided into three parts: the inner, middle and the outer archipelago, based on variations in their water exchange cycles, circulation and mixing (Engqvist and Andrejev, 2003). While Askö area is not officially part of the Stockholm Archipelago, it is likewise located in the Western Gotland Basin and shares similar water cycle dynamics observed in the middle and outer Stockholm Archipelago (Kautsky, 2008).

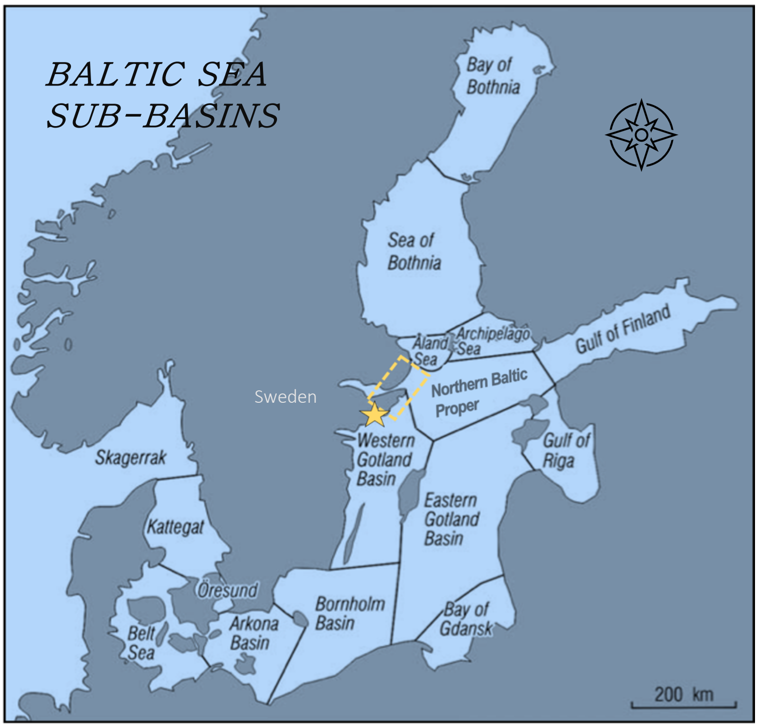

Figure 3. Map illustration of the Baltic Sea and its subbasin divisions. The general area of the Stockholm Archipelago is enclosed within a dashed, yellow rectangle. The Stockholm Archipelago extends over boundaries of the Northern Baltic Proper and Western Gotland Basin. Askö Island (58° 49' 21" N, 17° 38' 55" E) is marked as a yellow star, neighboring the southern margin of the Stockholm Archipelago. Askö Island lies within the Western Gotland Basin.

Image modified from Leppäranta and Myrberg (2009).

The Trosa and Stockholm Archipelagos are characterized as brackish-water archipelagos, heavily influenced by freshwater input from Lake Mälaren. Annual outflow from Lake Mälaren is estimated at an annual average discharge of 120 m^3/s (Jönsson, et al., 2005).

Due to the difference in salinity between outflow from Lake Mälaren and the saltier water of the Baltic Proper, a weak halocline forms separating surface and bottom waters. Mixing of the stratified water column is predominantly driven by surface winds and upwelling, with slightly strengthening intensity at the exposed margins of the southern archipelago (Hill and Wallström, 2008). Water flow is further limited by the topography of the Baltic Sea; In some regions, sills restrict water exchange between Baltic sub-basins, causing further variations in water composition and sedimentation regimes (Leppäranta and Myrberg, 2009).

Salinity fluctuations in the Askö area range between 6.3-7.7‰ at the surface and 8.7-10.3‰ below the halocline at approximately 100m depth (Leppäranta and Myrberg, 2009). Water surface temperatures vary from approximately 20°C in summer to 0°C in winter (Wiklund et al., 2012). The study area of this project also presents probable evidence for submarine groundwater discharge (SGD) in the form of terraces and semicircular depressions on the seafloor which possibly exert further influence upon water chemistry, circulation, and nutrient exchange in this region (Jakobsson et al., 2020).

2.2 Geological Setting

2.2.1 Regional Geology

The Askö region of the Baltic Sea lies within the Baltic Shield, also referred to as the Fennoscandian Shield (Šliaupa and Hoth, 2011). The basement is dominated mainly by Precambrian crystalline rocks thought to have initially metamorphosed ca. 1.95-1.75Ga BP following the Svecofennian orogeny during the Proterozoic Era (Tulling et al., 2011). Metamorphosed sandstones of Mesoproterozoic age (Jontian) can be found in neighboring regions, some with diabase dyke intrusions (*Figure 4a*) (Flodén and Winterhalter). Prior to the formation of the Jontian sandstones, rifting caused by post-Svecofennian granitic intrusions during the Middle Proterozoic (1.65Ga) allowed for the deposition and preservation of these sediments in tectonic depressions, as is the case for the nearby Landsort Deep (Tuuling et al., 2011), the deepest point in the Baltic at -459 m (Beckholmen and Tirén, 2008).

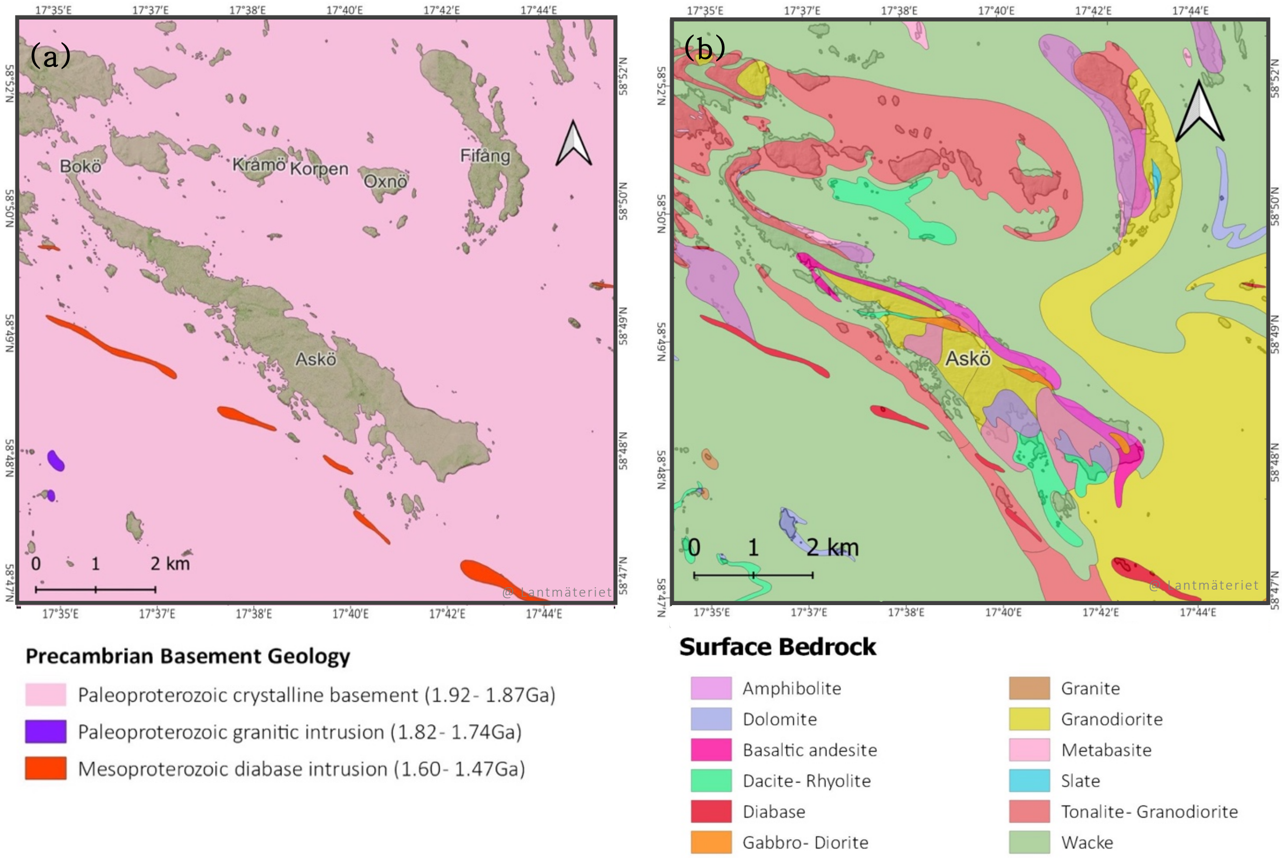

Figure 4. (a) Map of the study area showing the basement geology as color classified shapes. (b) Map of the study area displaying surface bedrock as color classified shapes. The geodata data used to create this map were provided by Lantmäteriet via the Swedish University of Agricultural Sciences (SLU) geodata portal. Visualizations are projected in Coordinate Reference System (CRS) SWEREF99 18 00, EPSG: 3011.

Askö primarily consists of metamorphosed igneous rocks, predominantly mafic or intermediate in composition. While there are small areas containing dolomite (a carbonate rock), they are less significant in comparison. The underwater geology of the region is primarily composed of sedimentary rocks, labeled as wackes in Figure 4b, with mafic intrusions running NW-SE along deformation zones. The tectonic folding illustrated in Figure 4b depicts the overall deformation of the study area, which allowed the formation of the islands as a result of tectonic compression or extension.

2.2.2 Formation of the Baltic Sea: A Summarized Timeline

The Baltic Sea is a relatively young intracontinental brackish sea which has undergone several stages during its short geological history. The formation of the Baltic Sea Basin began as an isostatically depressed area following the retreat of the extensive Saalian ice sheet covering northern Europe (Head et al., 2005), reaching its peak ca. 135 ka BP. Subsequent sea-level rise following deglaciation led to the inundation of the basin and the development of the Eemian Sea approximately 130ka BP (Eemian Interglacial) (Head et al., 2004). Marine paleoclimatic records reflect high climate variability following the initial stages of the then Eemian Sea, however definitive reconstructions of succeeding stadials and interstadials remain open for research (Andrén et al., 2011). More dynamic and well understood changes began to take place following the Last Glacial Maximum ca. 22ka BP. The developments leading to the modern Baltic Sea have been categorized into four main stages following the northward retreat of the Quaternary Late Weichselian glaciation (*Figure 5*).

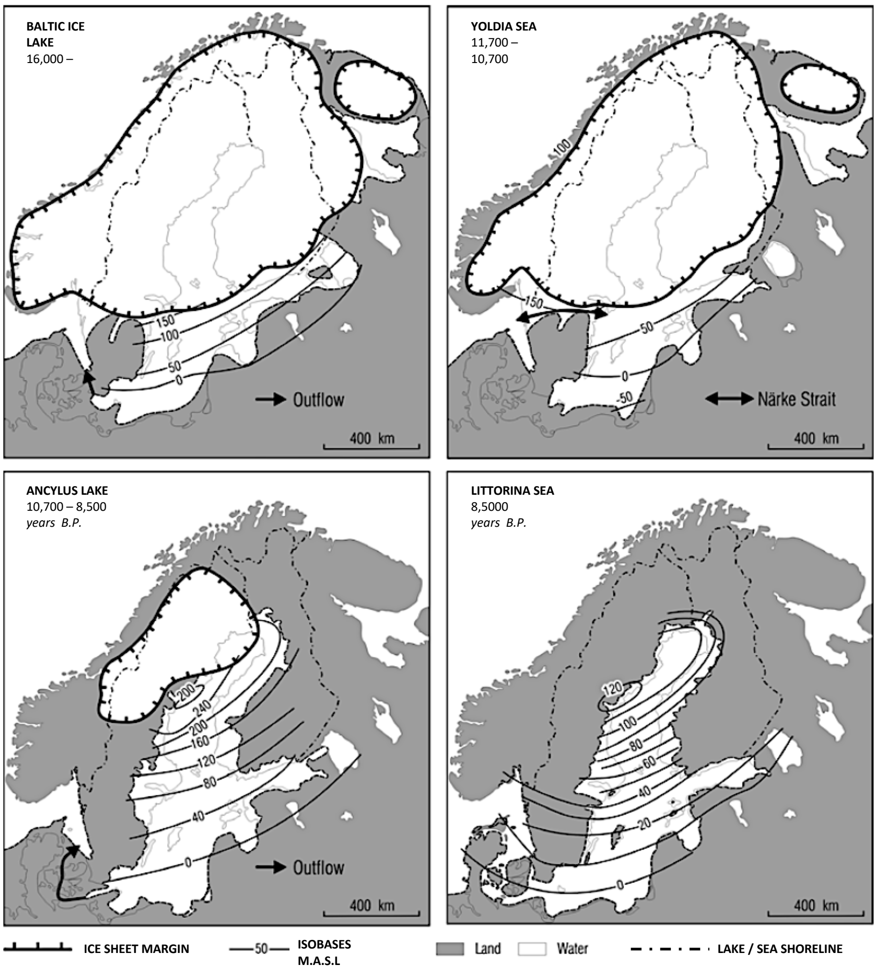

Figure 5. Illustrations displaying the four main stages of the Baltic Sea's formation. The Baltic Ice Lake (top left), Yoldia Sea (top right), Ancylus Lake (bottom left) and Littorina Sea (bottom right) are illustrated. The Baltic land area is shaded in gray and water & ice surfaces, in white. Contour lines indicate ice sheet margins, altitudes (from mean sea-level) and the extents of the sea/lake during each period. Black arrows point in the direction of water flow or drainage in the three initial stages.

The dates and durations of the four stages were collected from Leppäranta and Myrberg, (2009) and Andrén et al., (2011). Illustration modified from Leppäranta and Myrberg (2009), after Eronen and Haila, 1990.

Meltwater originating from the retreating ice sheet fed the proglacial Baltic Ice Lake (BIL), the first stage, ca. 16ka BP (Andrén et al., 2011). While the BIL was likely at sea level during the time of its formation, rapid isostatic rebound exceeded sea-level rise, and a freshwater ice-dammed lake took shape ca. 14 ka BP (Andrén et al., 2011). At approximately 13ka BP, further deglaciation exposed areas of the Swedish lowlands and provided a seaward route through Mount Billingen for the BIL to drain westward (Andrén et al., 2011). By ca. 12.8ka BP, readvancement of the ice sheet during the Younger Dryas stadial again blocked drainage to the open sea. The final phase of the BIL is marked by the "catastrophic" draining of the lake through Mt. Billingen, releasing ca. 7,800 km^3 of water at the end of the Younger Dryas cold ca. 11.7 ka BP (Jakobsson et al., 2007).

The Yoldia Sea (YS) marks the second stage of the Baltic Sea at ca. 11.7-10.7 ka BP (Head et al., 2005). Meltwater inflow following the Younger Dryas resulted in the rise of the Baltic sea-level. Rapid deglaciation caused an accumulation of postglacial sediment west of Lake Vänern, narrowing outlets leading seaward (Engqvist and Andrejev, 2003). Heavy outflow rates through these straights prevented saltwater inflow into the Baltic despite having contact with the open sea (Head et al., 2005).

At approximately 10.7ka BP, the Ancylus Lake (AL) stage began. This stage is characterized by a transition from freshwater to brackish conditions. Sea-level rise resulted in the expansion of the AL, eventually introducing saline water into the basin (Head et al, 2005). Evidence of weak saline water influence is dated at ca. 9.8ka BP. Finally, brackish water gradually began infiltrating northward, marking the end of the AL stage. During this time, the Scandinavian ice sheet had melted.

The final stage of the Baltic Sea began at ca. 8.5ka BP, the Littorina Sea (Head et al., 2005). The connection to the open sea via Öresund is believed to have expanded, allowing the flow of saline water into the Baltic (Head et al., 2005). A postglacial peak in salinity at approximately 6ka BP is thought to have been caused by lowered rates of freshwater input coupled with reestablished marine connection. Between 6-5ka BP, eustatic sea level rise significantly subsided while land uplift continued causing regression of the Baltic coasts. Consequently, salinity decreased. By 2ka BP, salinity reached levels comparable to the current-day Baltic Sea (Leppäranta and Myrberg, 2009). Currently, the Stockholm Archipelago region of the Baltic Sea experiences continued land uplift after the retreat of the Scandinavian ice sheet at a rate of approximately 5mm per year (Hill and Wallström, 2008).

The present-day Baltic Sea covers an area of around 415,266 km^2 with a water volume of 21,283 km^3 (Jakobsson et al., 2009). The Baltic Sea is classified as a shallow, brackish sea with a depth mean depth of 54m (Leppäranta and Myrberg, 2009).

3. FUNDAMENTAL CONCEPTS

3.1 Principles of Acoustic Geophysical Mapping

The mechanisms and interactions involved in acoustic geophysical mapping are intricate and numerous. The following introductions are succinctly summarized and focused on core principles necessary for general understanding. While there are various methods and instruments available for performing surveys, the descriptions presented are those relevant to the instruments used for this project. Some essential and elaborate components, such as navigation and geopositioning systems are given limited attention.

3.1.1 Echo Sounding

The fundamental principle of underwater acoustic surveying is *echo sounding* – the transmission, propagation, and interpretation of underwater sound waves. During the process of echo sounding, a *transducer* generates an underwater sound pulse which travels through the water column and reaches the seafloor. The acoustic pulse then "echoes" from the seafloor and is detected by a *receiver*. By measuring the time it takes for a transmitted pulse to reach the seafloor and return to a receiver (TWT), the depth (D) of the seafloor can be determined as seen in (1). Knowledge of the speed of sound (v) through the water column is essential in this calculation.

$$D = v \times \frac{\text{TWT}}{2} \quad (1)$$

3.1.2 Underwater Speed of Sound

The speed of sound in the ocean is determined by water's physical properties. The density (ρ) and compressibility or *bulk modulus* (K) of water control the propagation speed of sound waves emitted during echo sounding (Jakobsson et al., 2016). Underwater sound speed can be calculated as seen in (2).

$$v = \sqrt{\frac{K}{\rho}} \quad (2)$$

The composition of water across seas and oceans is not constant which results in variations of the speed of sound throughout time, locations, and depths. The primary factors influencing the speed of sound in seawater are pressure, salinity, and temperature. In stratified bodies of water, the speed of sound will naturally fluctuate as a pulse moves through layers of the water column with different compositions. On average, the speed of sound in saltwater is approximately 1500 m/s and salinity ranges between 32 to 38 ppt in the open ocean (Jakobsson et al., 2016). Changes in salinity of 1 ppt cause an approximate change of 1.3 m/s in sound velocity. With increasing pressure due to depth, sound velocity increases 0.017 m/s for every meter (Jakobsson et al., 2016). As temperature decreases with depth in the open ocean, sound velocity will decrease 2.5-4.7 m/s for every degree (Jakobsson et al., 2016). To accurately interpret bathymetry and geological features through echo sounding, a sound velocity profile (SVP) needs to be calculated to correct for the aforementioned factors. The Mackenzie formula, developed by Kenneth V. Mackenzie (Mackenzie, 1981), is one of the most commonly used empirical equations for this purpose (Jakobsson et al., 2016). The equation calculates the speed of sound (v, m s−1) based on temperature (T, °C), salinity (S, ppt) and pressure as depth (D, m) as seen in (3). The range of validity for this equation is water temperature of 2 – 30°C, salinity of 25-40 ppt and depths between 0-8000 m (Mackenzie, 1981).

$$\begin{aligned} v = {} & 1448.96 + 4.591T - (5.304 \times 10^{-2})T^2 + (2.374 \times 10^{-4})T^3 \\ & + 1.340(S - 35) + (1.630 \times 10^{-2})D + (1.675 \times 10^{-7})D^2 \\ & - (1.025 \times 10^{-2})T(S - 35) - (7.139 \times 10^{-13})TD^3 \end{aligned} \tag{3}$$

Sound velocity observations can be made by deploying sound velocity probes during a survey. Conductivity-Temperature-Depth (CTD) sensors are one example of the standard instruments used for this purpose. CTDs are lowered and raised from the survey vessel by a cable-mounted frame and continuously measure conductivity (salinity), temperature and pressure as they move through the water column (Jakobsson et al., 2016). This data is commonly visualized in graphs, with lines depicting the values for each parameter through the depth of the measured water column.

Sound waves move longitudinally through water (*acoustic media*) in the direction of the propagation of the wave (angle of incidence). As an acoustic signal travels through the water column, it will *refract* when encountering layers or media with different sound velocities. "Some of the energy is *reflected* at the interface with the same angle as the angle of incidence and some continues to propagate into the second medium". (Jakobsson et al., 2016). This phenomenon is described by Snell's Law equation as seen in (4), where θ_1 represents the angle of incidence, θ_2 represents the angle of refraction and v_1 and v_2, the sound speeds in each layer.

$$\frac{\sin \theta_1}{v_1} = \frac{\sin \theta_2}{v_2} \tag{4}$$

Refraction will cause sound waves to bend towards or away from the interface, depending on the speed of sound at each layer. For example, refraction due to sound wave moving from a layer of high speed to one of lower speed will result in a downward bending of the sound pulse (*Figure 6*). This interaction can produce errors or artefacts in the data produced by echo sounders. SVP measurements can be used to correct the angles caused by refraction and calculate the true trajectory of the acoustic beams, in a process called *ray tracing.*

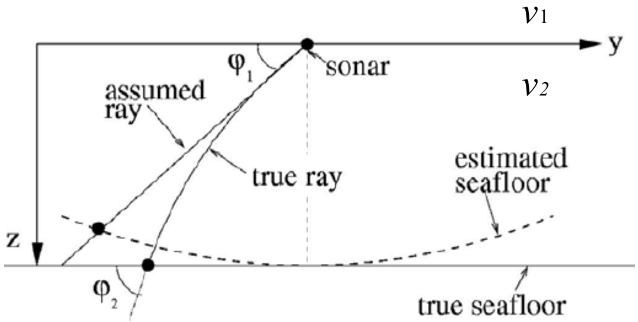

Figure 6. Schematic diagram showing the effect of soundwave refraction. Θ_1 represents the angle of incidence and Θ_2 represents the angle of refraction. '*Y*' corresponds to the interface between two media with different impedances, represented as V_1 and V_2. When the speed of sound is greater in V_1 than V_2, the ray path bends away from the interface, as seen here. Inversely, the ray will bend towards the interface when $V_2 > V_1$.

3.1.3 Multibeam Echo Sounder

MBES have rapidly become the tool of choice for creating bottom habitat maps due to their ability to simultaneously collect georeferenced bathymetry and backscatter data (Kenny et al., 2003). MBES systems emit across-track sound pulses from hull-mounter transducers. Several pulses make up a fan or *swath,* of conical beams transmitted towards the seafloor. Receivers arranged along-track (along-keel) collect the returned acoustic pulses reflected from the seafloor. The area where the transmitting and receiving beams intersect is referred to as the sonar *footprint* in a *Mills Cross or Mills T* sonar arrangement (Jakobsson et al., 2016) *(Figure 7)*.

The resolution achievable by MBES systems is determined by the geometry of the transducer's aperture, the depth surveyed, and the wave frequency transmitted (*Table 1*). The transducer's arrangements, vessel's positioning accuracy are also among the numerous factors that influence the quality of the acquired data.

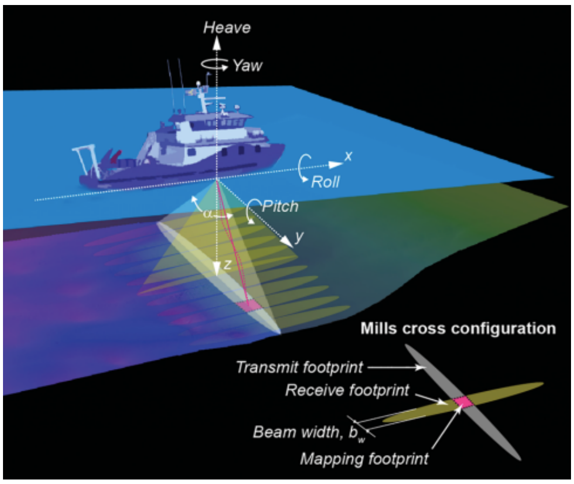

Figure 7. Illustration of MBES configuration displaying the Mills cross arrangement and vessel position variables, such as the pitch (y), roll (x), heave and yaw.
Image from Jakobsson et al., 2016.

Depth Range (m)	Frequency (kHz)	Wavelength (cm)
< 100	> 200	< 0.75
100 - 1500	50 - 200	3 – 0.75
> 1500	12 - 50	12.5 - 3

Table 1. Common operating parameters for MBES as defined by the International Hydrography Organization (2015).

When selecting a MBES system for the purpose of habitat mapping, it is important to consider the size of the area to be covered, the depth ranges to be surveyed and necessary resolution (Kenny et al., 2003).

3.1.4 Acoustic Backscatter

Bathymetry indicates *where* the seafloor lies, however, backscatter displays *what* it consists of. Backscatter values are notated in *decibels (dB)*, representing the intensity of recovered acoustic signals from the surveyed seafloor.

The acoustic signals emitted from the multibeam sonar system reach the seafloor at an angle. This wavefront will scatter in multiple direction depending on the hardness of the seabed encountered (Fonseca and Mayer, 2007). The angular dependence of the backscatter signal results in high BS intensities at the vertical (below the nadir) and decreasing intensities with increasing incident angle (*Figure 8a*). This is true for soft sediments (*Figure 8b*). However, hard or coarse sediments will scatter the sound waves in all directions and show little dependency on changing incident angles (Figure 8c) (Lurton et al., 2015). The character of this returned signal provides valuable information about the physical properties of the seafloor. Using this information, the seafloor can be sectioned into areas displaying similar acoustic properties (Fonseca et al., 2008).

Backscatter intensities recorded by MBES systems are also influenced by additional factors, such as the sonar frequency, and characteristics of sonar beam pattern. To utilize backscatter signals for seafloor classification, geometric and radiometric corrections need to be made. The signal is corrected geometrically for the angle of incidence and beam pattern. Radiometric corrections account for pulse length and the receiver's bandwidth (Lamarche et al., 2011). These corrections are performed by mathematical models and algorithms and are further described in this project as the selected method for seafloor characterization.

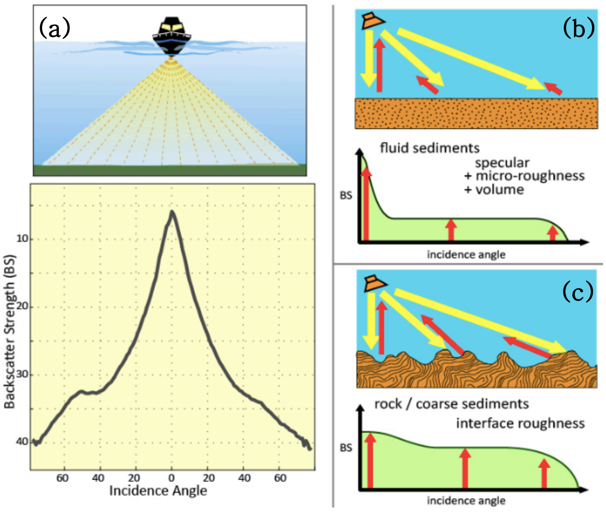

Figure 8. **(a)** Illustration of the angular dependence of BS strength in soft sediment **(b)** and hard seabed **(c).**

Image from Lurton et al., 2015.

3.2 Bottom Habitat Mapping

While the term *habitat* is most frequently associated with living organisms, it is also commonly used in the field of acoustic mapping to describe the spatial distribution of distinct seafloor characteristics (Brown et al., 2011). The expressions "*bottom* habitat mapping" and "*benthic* habitat mapping" in this project when discussing seabed sediment mapping.

The process of creating benthic habitat maps often combines various marine science disciplines to interpret, define and produce accurate representations of the seafloor (Brown et al., 2011). In the context of geophysical mapping, benthic habitats are generally defined by sediment type and distribution, throughout a surveyed area of the seafloor. These classifications provide insight into underwater seabed processes and can serve as valuable tools for monitoring changes in marine ecosystem, establishment of protected areas, as well as the growing effects of anthropogenic disturbances (Walton et al., 2016). The classification methods used for creating seabed habitat classifications depend on the discipline and intended purpose of individual studies. Because of this, there is no standard approach to data collection methods.

Generally, in-situ sampling when conducting these studies is expected. Samples or *ground truths*, can be collected in the form of sediment grabs and coring as well as visuals recorded by remotely operated (ROV) or autonomous underwater vehicles (AUV). In-situ investigations can also be made by divers, such as video and photographs, at locations where sea depths allow. The properties of the collected sediments and observations made from video recordings are used to compliment the acoustic data acquired by sonar instruments.

4. MATERIALS

4.1 Data Acquisition

The data acquisition surveys compiled for this project were conducted on Stockholm University's *R/V Electra* and *R/V Skidbladner*. Most of the surveys were performed as part of Stockholm University's yearly course in geophysical mapping. In addition, data acquired by Jakobsson et al., (2020) during research surveys of the region is also used in this study. Both research vessels utilized Kongsberg EM2040 multibeam echo sounders to produce high-resolution bathymetric data of Askö region (*Table 2a*). Positioning and navigation data was recorded by a Seapath 330+ navigation system with real-time kinematic (RTK) correction. Horizontal and vertical accuracies of 2-3cm and 4-6cm respectively, can be achieved by this system. Sound velocity readings were performed using a combination of hull-mounted sensor and manually deployed sound velocity probe (*Table 2b*). The surveys were conducted from 2012 to 2022, primarily between the months of May and October.

Table 2a.

Vessel	Size	MBES	Sensor Location	Transducer Geometry	Operating Frequency	Depth Range	Navigation System	Source Satellites
R/V Electra	24.3 x 7.2 m	Kongsberg EM2040	hull-mounted	0.4° X 0.7°	200-400 kHz	0.5 – 550m	Seapath 330+; RTK	GPS, GLONASS
R/V Skidbladner	6.4 x 2.4m	Kongsberg EM2040	pole-mounted	1° x 1°	200-400 kHz	0.5 – 550m	Seapath 330+; RTK	GPS, GLONASS

Table 2b.

Sound Velocity Sensor	Placement on Vessel	Reading Rate & Location
AML Oceanographic	hull-mounted	continuous; surface speed
Valeport MiniSVP	deployed	discrete; at depth

Table 2. (a) Specifications of the surveying instruments onboard *R/V* Electra and *R/V* Skidbladner. (b) Details of vessel placement and operating mode of the sound velocity sensors used during the surveys in this project.

4.2 In-Situ Investigation

4.2.1 Core Samples

Throughout the course of the data acquisition surveys, several sediment core samples were extracted from the eastern Askö seafloor. The sediment cores were retrieved aboard *R/V Electra* by a piston-gravity coring system specifically adapted for this vessel (Jakobsson et al., 2020). These cores were studied and described by students at Stockholm University for a variety of projects and reports. Information about the core samples which fell within the study area were compiled from these reports and used to compare the software generated sediment characterization to the observed ground-truths (Table 3). Only the core descriptions which included the surface layer of sediments were selected for this comparison.

Table 3.

Coordinates	Core ID	Segment Depth (below seafloor)	Student Report
17.68607, 58.85145	Asko2017HT-02gc-1	0-31.5 cm	Ghasemi, F., 2018.
17.69556, 58.85861	2010-PC2	0-10 cm	Hjalm, K., 2013.
17.68056, 58.85194	2010-PC3	0-29 cm	Hjalm, K., 2013.
17.69139, 58.82472	2009-PC3	0-10 cm	Hjalm, K., 2013.
17.70290, 58.83730	EL20-IGV07-2PC-SEC2-0-3	0-99 cm	Lindström, M., 2022.

Table 3. Details of the sediment cores used in this project. Core names, locations, depths are listed along with the student reports in which the sediments were described.

4.2.2 Dive Sites

During research conducted by Jakobsson et al., (2020), divers captured video and photographs of areas east of Askö / west of Fifång where underwater terraces are present in the seafloor morphology. The captured footage was used in this study as visual confirmation of the remotely resolved landforms in the processed hydroacoustic data.

5. METHOD

5.1 Geophysical Data Processing

The multibeam bathymetry surface used as reference during backscatter processing is from Jakobsson et al., (2020). They used Qimera version 1.7.2, of the QPS software suite. A bathymetric grid with a resolution of 1x1m was compiled by Jakobsson et al., (2020). This grid was imported to QPS's Fledermaus Geocoder Toolbox (FMGT) software, version 7.10.2 and used in this study to compare backscatter features to the underlying bathymetry (*Figure 9*). The seafloor depth measurements offered by this grid were also used to create the bathymetric map of the study area, seen in Figure 2.

The backscatter data simultaneously acquired during the multibeam mapping surveys was processed and gridded solely on FMGT. Open-source graphic information system QGIS, version 3.22.14 Bialowieza was used for visualization and post-processing analysis of the backscatter mosaics generated on FMGT.

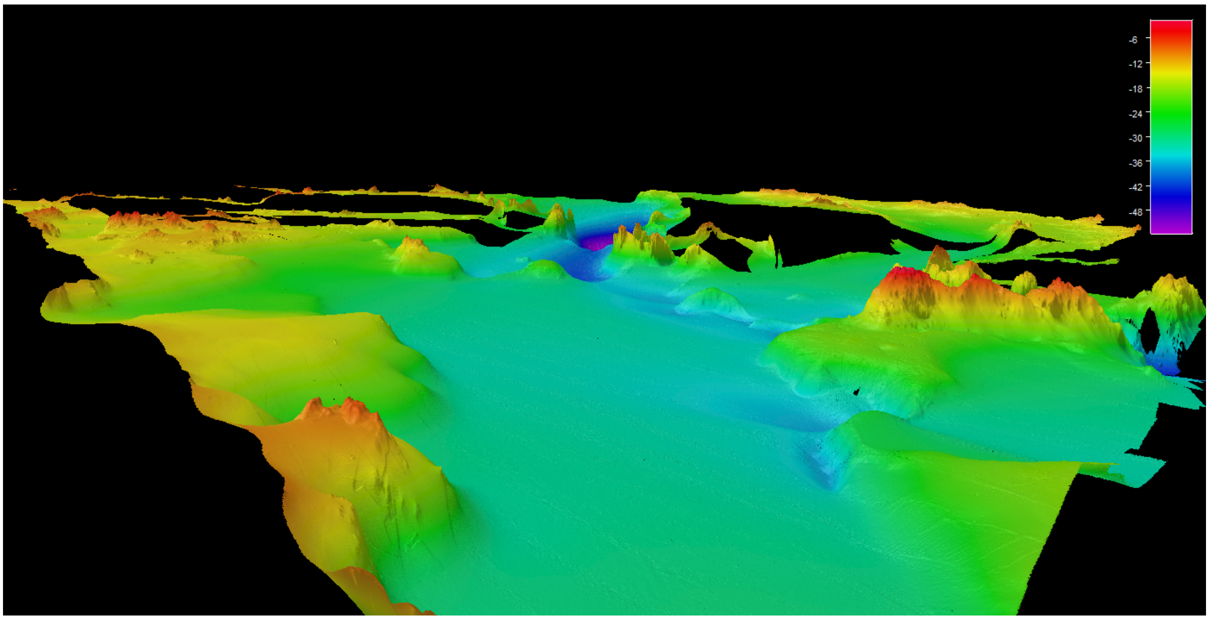

Figure 9. Screen-captured image of a digital terrain model and accompanying bathymetry of the east of Askö Island, as displayed on Qimera. This surface was created by Jakobsson et al., (2020). Depth ranges are projected as a color scale, with purple (-54 m) and deep blues representing greater depths and red areas (-2 m) corresponding to shallow peaks. The grid can be rotated 360° on Qimera, for a complete view of seafloor features. This captured image faces roughly northwest, looking towards Fifångsdjupet.

5.1.1 FMGT

FMGT was the primary data processing software used for this project. A total of 233 source files in Kongsberg's raw .all format were imported, containing backscatter data recorded by each mapped survey line. The source files used WGS84 as geographic reference and were projected using SWEREF99 18 00 + RH2000 height. Sound velocity profiles obtained during the mapping surveys and system configuration information were automatically included in these files. Processing was initially carried out using default parameters, including automatic radiometric corrections according to the used sonar system as well as angle varying grain (AVG) adjustments to reduce noise and variations in the backscatter levels. Some processing settings were later adjusted to minimize errors and artefacts.

Individual backscatter measurements were combined during processing resulting in software generated *mosaics*, or visual representations of the backscatter values throughout the surveyed seafloor. Based on the source data provided, FMGT automatically computed a resolution of 0.2x0.2 m per pixel within a survey area of approximately 45 km^2. In order for the computer to manage the mosaic's memory requirements, the backscatter mosaic was partitioned into twelve *tiles*, each measuring 2x2 km (*Figure 10*). This division facilitated the handling of the mosaic data by the computer and helped in minimizing subsequent processing time while rendering adjustments.

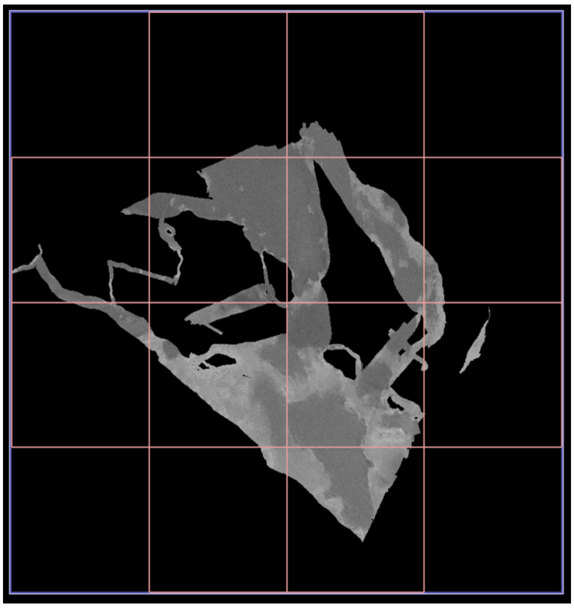

Figure 10. Screen-captured image of the mosaic tiles (pink-orange lines) created on FMGT, atop the backscatter mosaic.

Following this process, three mosaics were created, representing: backscatter intensity, statistics, and Angle vs. Range Analysis (ARA) based sediment characterization.

5.1.1.1 *Errors and Corrections*

Following the initial stage of processing, errors were clearly visible in the backscatter mosaic. Corrupted or incomplete source files caused distortions during the rendering process. The distorted segment (visualized as static lines across the nadir), were manually selected using the *Edit Selection Tool*, and removed (*Figure 11*).

Figure 11. Screen-captured FMGT image showing data processing errors in the backscatter mosaic circled in red. The red and green lines across the distorted backscatter represent the port and starboard beam swaths along the track line's nadir (white lines).

Other processing issues resulted from the joining of data acquired by two different vessels or during various surveys. This resulted in boxy patches of ununiform backscatter values in sections where the survey lines overlapped (*Figure 12*). FMGT provides tools for *Intra-Vessel Backscatter Adjustment*, however, since the data was acquired using equivalent systems and frequencies, the software did not recognize any dissimilarities. Instead, manual data corrections were performed to adjust backscatter levels in survey lines that did not match the surrounding values.

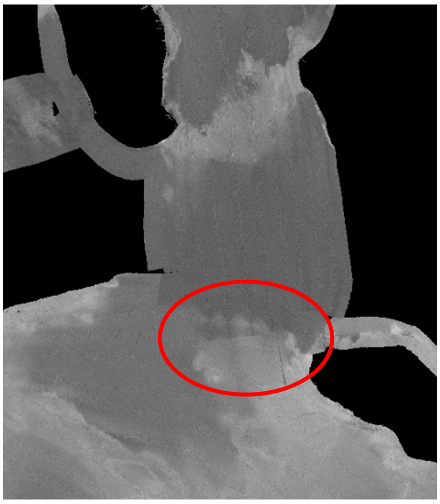

Figure 12. Screen-captured FMGT image showing data processing errors in the mosaic, circled in red. These boxy patches likely resulted from the joining of data from multiple surveys (with different backscatter intensity values for the same area).

These discrepancies were corrected using the Cascading Backscatter Normalization tool to normalize backscatter differences between survey lines. The "problem lines" were selected along with a reference line to balance them against (*Figure 13*). The backscatter levels were then adjusted based on the dB offset computed by the tool. This process worked for many of the uneven segments, but some survey lines required manual adjustment of the backscatter levels. Such adjustments were made using the Line Backscatter Adjustment tool to visually match the segments to the surrounding survey lines.

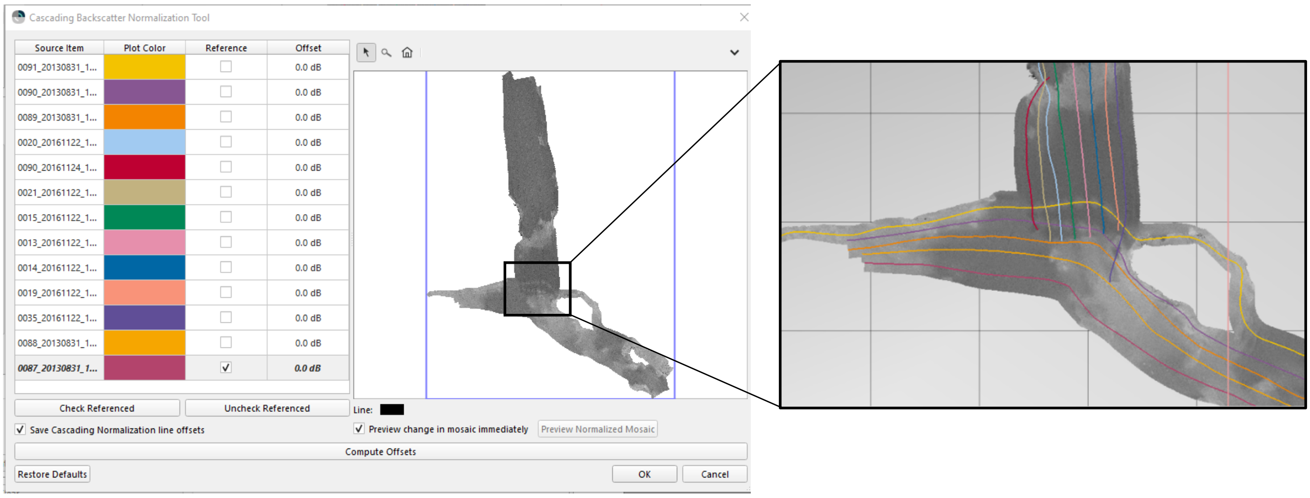

Figure 13. Screen-captured image of the *Cascading Backscatter Normalization Too*l used on FMGT to correct the boxy patches seen in Fig. 12. Thirteen lines were selected to normalize the "problem track" against. The picture on the right shows the corrections made in the area's backscatter (outlined by a black box) after using this tool,

Strong artifacts were also visible as pixelated lines at the nadir throughout the length of the survey tracks. These artifacts reflect the higher values at lower incidence angles (below the nadir) and decreasing values at greater angles (away from the nadir) (Fonseca et al., 2009). Mosaicking parameters were adjusted to *Fill gaps using adjacency* to reduce the nadir in the rendered mosaics. Other available options were explored but resulted in undesirable modifications with further distortions. While the effect of the nadir was significantly reduced, the striping pattern from the nadir artifacts could not be removed entirely and remains visible in the adjusted mosaics.

Once the backscatter data were processed and adjusted to a satisfactory level, final Backscatter, Statistics and ARA layers were created.

5.2 Visual Objects

5.2.1 Backscatter Mosaic

The generated mosaics appear in FMGT under *Visual Objects*. The *Backscatter Mosaic* was the primary object used for identification of geomorphological features of the seafloor. The mosaic was displayed as a grayscale surface representing backscatter intensity levels, or reflectivity, measured in decibels (dB). As previously established, the backscatter strength (BS) is a function of the incident angle of the acoustic signal at the seafloor. By applying Angular Varying Grain correction, grazing angle variations are normalized during processing (Fonseca et al., 2009). The original incidence angle information is stored by FMGT for later use. Seafloor composition and roughness also influence the strength of the returned signals. With the grayscale visualization scale applied in this work, bright areas correspond to seafloor features with higher reflectivity while darker areas indicate greater absorption. The Backscatter Mosaic was exported as a grayscale GeoTIFF (.TIFF), later used for mapping visualization.

5.2.2 Statistics Layer

It is important to note that while the visual layers are created at once during processing, every visual object generated follows a processing pipeline in which the values are dependent on each of the previously created mosaic/layer. For the *Statistics layer*, FMGT automatically conducts statistical analysis on the backscatter values produced by the Backscatter Mosaic. The resolution of the Statistics layer is by default 20 times the resolution of the Backscatter Mosaic. In this case, the statistics were resolved to 4x4 m pixels. While the statistical analysis generates various products, only the layer containing the mean backscatter values was used for interpretation and visualization. This layer was exported as a color GeoTIFF (.TIFF) raster as well as comma separated statistical values (.csv).

5.2.3 ARA Layer

Finally, the Angle vs. Range Analysis (ARA) layer was generated with a resolution of 4x4 m. The ARA algorithm creates rasterized cells, port and starboard of the survey tracks representing two distinct patches of the seafloor. For this layer, FMGT uses incidence angle information and characteristics of backscatter signal to interpret the properties of seafloor sediments (Fonseca et al., 2009). Angle vs. Range Analysis compares the recorded backscatter to mathematical models of expected acoustic response, according to the instruments and parameters used during surveying. The generated classifications are a function of the grazing angle vs. returned backscatter intensity (Fonseca et al., 2009). Seafloor properties such as acoustic impedance, roughness, volume (density and porosity), sediment type and grain size were estimated by FMGT through this process. No manual adjustments were made to the generated ARA Characterizations.

The Characterization layer cataloged sediments on a scale of 1-20, ranging from gravel to clay (*Table 4*). These software generated classifications can be manually edited according to grain size (mm) or by realigning the characterization model bounds to follow the recorded beam pattern angles of an individual seafloor patch (*Figure 14*). Other properties can also be adjusted, such as sediment porosity and permeability, and corrections can be applied to the entire survey area or individual portions along a track line.

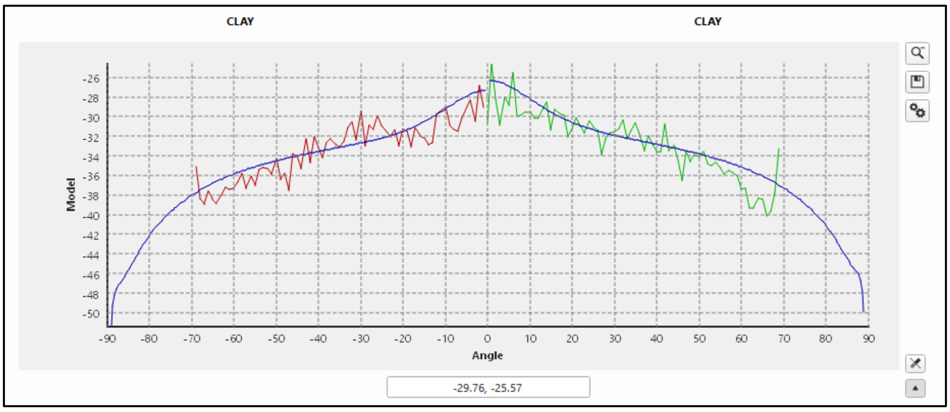

Figure 14. Screen-captured image of FMGT's *Angle vs. Range Analysis Dialog* window. Port and starboard beam patterns are displayed as red and green plotted lines, respectively. The blue curve represents the characterization model parameters, in this case, identifying the sediments in this patch as clay.

This range loosely follows Folk's sediment classification scheme (Folk et al., 1970), which is displayed as ternary diagrams of sediment ratios (*Figure 15*). Folk's sediment classification scheme is one of several parameters used by the International Organization for Standardization (ISO). The ISO makes use of Folk's scheme for sediment size, Shepard's "sand-silt-clay ratios" (1954) for size class proportions and

Albert Atterberg's (1846-1916) "Atterberg limits" based on the water content in cohesive soil, among others, to set industry standards. However, the exact classification parameters used by hydroacoustic data processing software are proprietary algorithms and are seldom revealed in their entirety.

The ARA layer was exported as a pseudo-color GeoTIFF (.TIFF) raster and comma separated values (.csv).

Table 4.

	ARA Characterization	Grain Size (mm) *Folk et al., 1970*		Table 4 Continued	
1	gravel	>2	11	clayey sand	-
2	gravelly coarse sand	2 - 1	12	coarse silt	0.0625 – 0.031
3	coarse sand – sandy gravel	1 - 0.5	13	sandy silt	-
4	coarse sand – gravelly sand	-	14	medium silt	0.031 – 0.0156
5	medium sand – gravelly muddy sand	-	15	sandy mud	-
6	medium sand	0.5 – 0.25	16	fine silt	0.0156 – 0.0078
7	fine sand	0.25 – 0.125	17	sandy clay	-
8	silty sand	-	18	very fine silt	0.0078 – 0.0039
9	muddy sand	-	19	silty clay	-
10	very fine sand	0.125 – 0.0625	20	clay	< 0.0039

Table 4. Sediment classifications according to Folk et al. (1970), alongside the corresponding ARA characterizations.

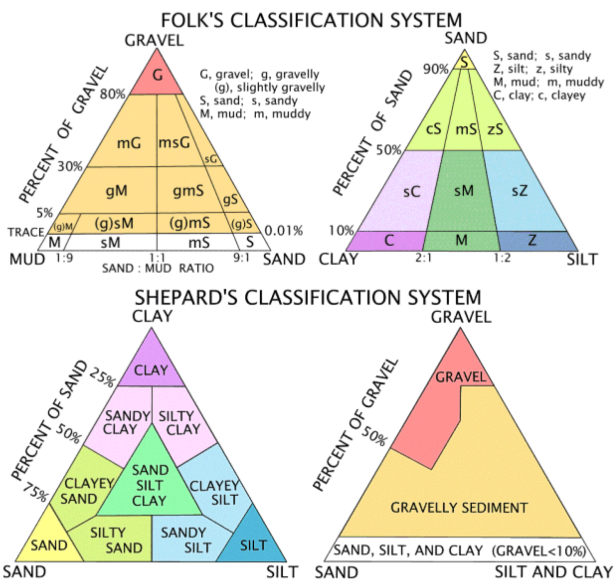

Figure 15. Ternary diagrams of Folk's and Shepard's sediment classification systems, two of the commonly used class schemes. Image retrieved via The Planetary Society, URL: planetarysociety.org

5.3 QGIS

The generated visual objects were imported to QGIS as rasters and displayed in maps of the study area. A vector (point) layer including the location and information of in-situ investigations was also created using this software.

The .csv file containing coordinates and corresponding classification was imported to QGIS. The ARA Characterizations were listed on a scale of 1-20, along with the coordinates for each value. This data was converted into a raster for visual interpretation of the data. The sediment classification layer was later interrogated at the locations (points) where core samples were extracted, to determine if the software generated interpretations correlated to the ground-truth data. Chatbot Generative Pre-trained Transformer (ChatGPT) language model from OpenAI was used during the map making process, to correct and generate data visualization equations as well as data analysis commands.

Maps displaying the Backscatter Mosaic, Statistics, ARA Characterization and resulting Bottom Habitat maps were projected using Coordinate Reference System (CRS) SWEREF99 18 00, EPSG:3011.

6. RESULTS

The results for this study are presented in the form of georeferenced maps, displaying individual visual layers created on FMGT. The first three maps show the Backscatter (*Map 1*), Statistics (*Map 2*) and ARA (*Map 3*) layers, in the order which they were created by the processing software. Finally, Bottom Habitat Maps (*Map 4 & Map 5*) are presented, displaying sediment classes defined by discrete colors.

6.1 Maps of Visual Objects

6.1.1 Backscatter Mosaic

The backscatter mosaic is resolved to 0.2x0.2m. Backscatter strength ranges between a high of 10dB to low of -70dB, visualized as bright and dark regions respectively. The lowest backscatter levels are found at the deepest areas and expand northward where the seafloor continues uninterrupted by islands.

Distinct seafloor features can also be observed, particularly those found closest to southwestern shores of Fifång Island. A concentration patterns resembling steps, are brightly marked on the seafloor. In the central survey area, intermediate backscatter values are immediately surrounded by “shelves” with higher backscatter intensity. At points where this contrast is most pronounced, seafloor depths quickly drop approximately 10m in less than 40m. In areas where changes in intensity are gradual, the seafloor depths increase, gently sloping towards the center.

6.1.2 Statistics

During the processing of the backscatter data, mean backscatter values for the entire survey area were automatically computed and detailed in the Statistics layer. The statistical analysis performed by FMGT includes mean, minimum and maximum values as well as skewness, kurtosis, standard deviation, grazing angle and number of samples (among others). However, for the purpose of this study only mean values were used. These values were presented in two formats: a visual layer, shown in the Statistics Map, and as comma-separated values. The dataset included precise coordinates for each value, recorded at 4x4 m intervals. The resulting dataset comprised 747,499 values indicating a mean range of backscatter levels between 4dB and -64dB across the seafloor. Analysis of the data revealed that the most frequently occurring backscatter level was -36dB, covering 1.5 km^2 of the study area.

6.1.3 ARA Characterization

Following the processing of backscatter data, FMGT generated layers based on geometric and radiometric corrections made. The ARA Map below uses the "Characterization" layer, which classifies seafloor sediments by grain size. However, visual layers indicating seafloor impedance, roughness, depth, and fluid factor (among others), are also produced. It is through the analysis of each of these properties, that seafloor sediment types are determined by the software.

According to this categorization, large expanses of the study area's seafloor surface are composed of clay (red). Areas with low backscatter intensities and greater depths (as seen in *Map 1*), are classified as fine sediments.

6.1.4 Bottom Habitat Maps

Sediment classes were assigned by characterizations estimated during the data processing phase. In other words, the Bottom Habitat maps represent the discrete values produced by the ARA analysis to display bottom sediments as individual, color-coded classes. The Generalized Bottom Habitat map unites sediments by their primary composition, displaying them as groups or general types.

The maps illustrate that the surveyed seafloor primarily consists of clay and fine sediments. The areas exhibiting high backscatter values in the BS mosaic (*Map 1*), are interpreted as coarse sediments such as "gravel" or "sand". This is markedly true for the channels between small islands and near the shorelines.

The deepest parts of the study area are largely classified as fine sediments. In the central region, there is a distinct contrast in sediment types, mirroring the intensity variations observed in the BS mosaic. The "clay" and "silt"-covered seafloor is surrounded by areas of "coarse sand" and "gravel". In most of this region, sediments gradually decrease in grain size from island margins towards the center.

BACKSCATTER MOSAIC

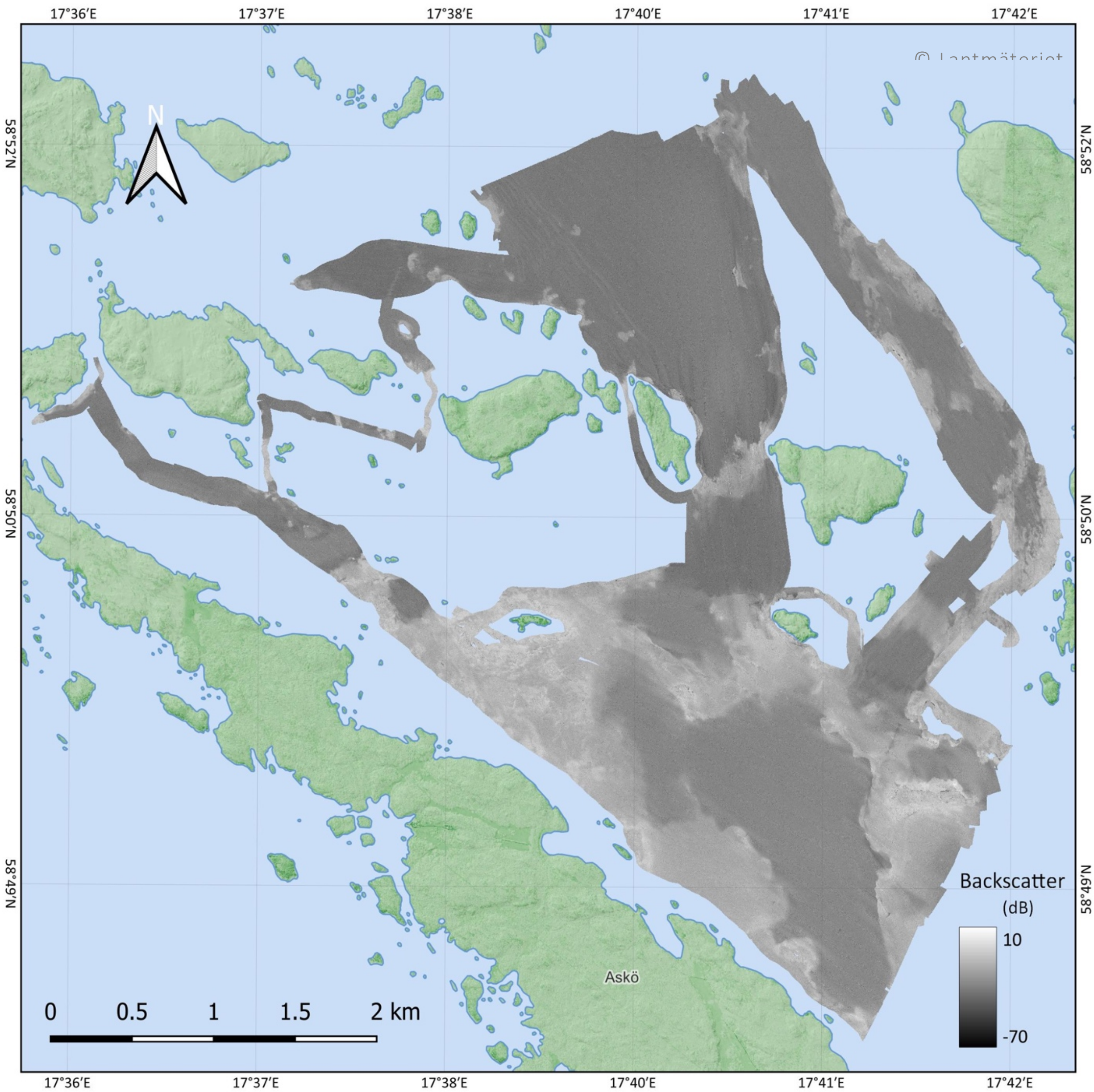

Map 1. Visualization of backscatter intensity levels generated by FMGT, on the eastern seafloor of Askö Island. Backscatter strength ranges between a high of 10dB to low of -70dB, at a resolution of 0.2x0.2 m.

The geodata data used to create this map were provided by Lantmäteriet via the Swedish University of Agricultural Sciences (SLU) geodata portal. Visualizations are projected in Coordinate Reference System (CRS) SWEREF99 18 00, EPSG: 3011.

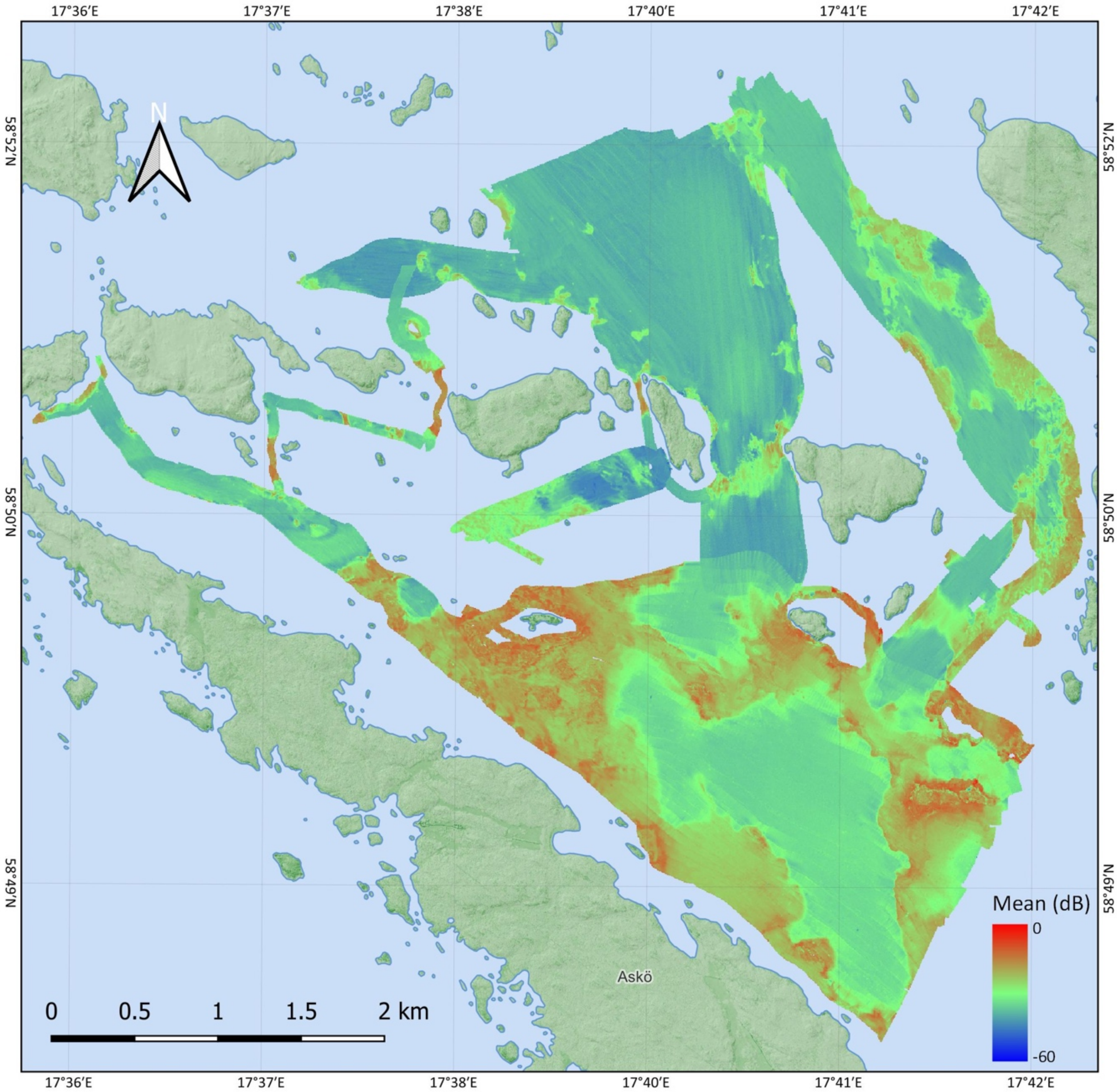

Map 2. Mean backscatter intensity levels east of Askö Island, displayed using a pseudo-color scale. Mean values range from a high of 10dB to a low of -60dB. The statistics layer is resolved to 4x4 m.

The geodata data used to create this map were provided by Lantmäteriet via the Swedish University of Agricultural Sciences (SLU) geodata portal. Visualizations are projected in Coordinate Reference System (CRS) SWEREF99 18 00, EPSG: 3011.

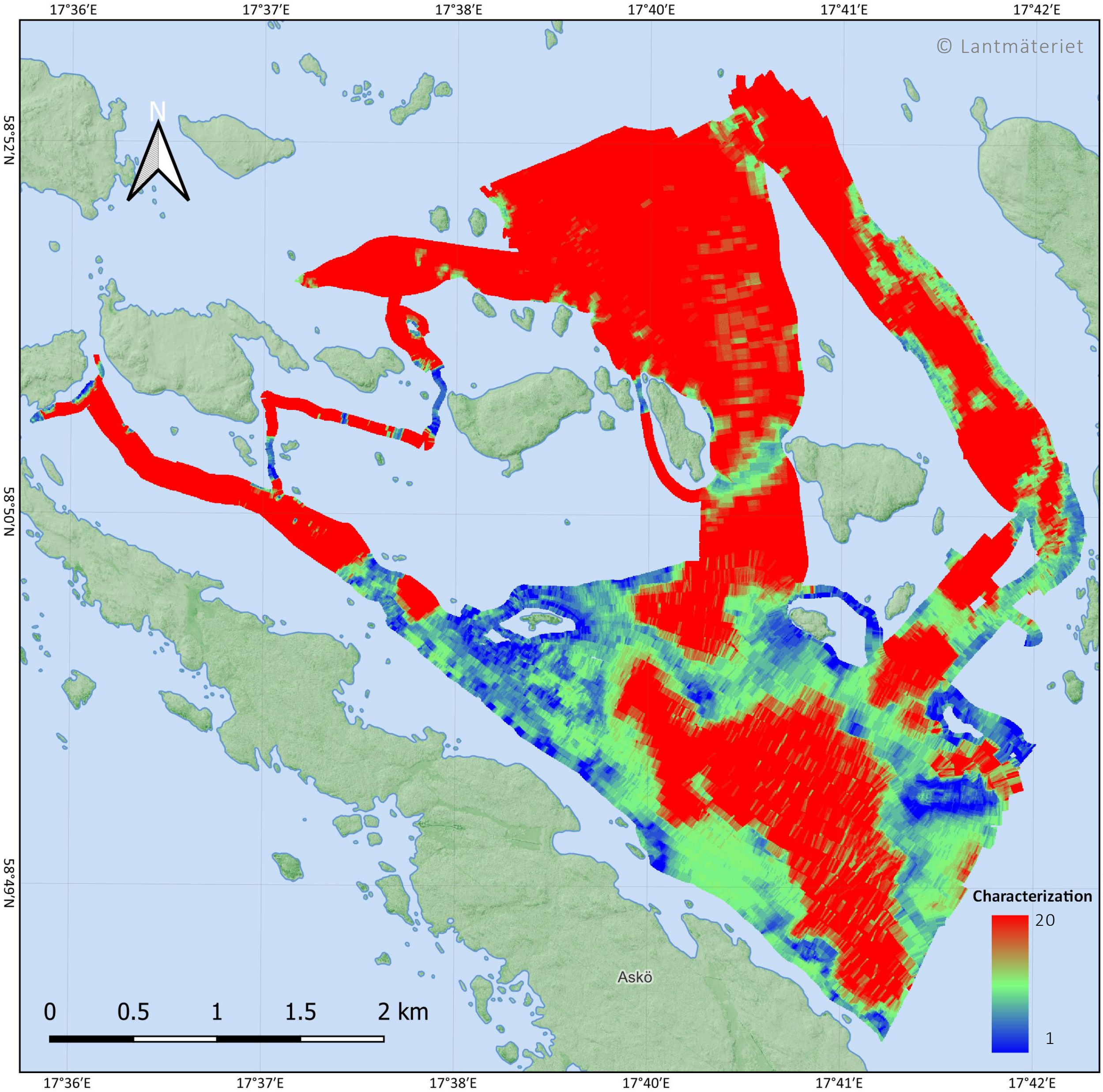

Map 3. Georeferenced raster image of the estimated bottom sediments east of Askö island. The characterization is displayed as a spectral signature, with values corresponding to the sediment classes assigned by FMGT. A value of 1 (blue) represents gravel or coarse sediments while 20 (red) represents fine sediments or clay. The ARA layer is resolved to 4x4m and projected using CRS EPSG:3011. The satellite imagery and additional geodata used to create the basemap was collected by Lantmäteriet and downloaded via the SLU geodata extraction portal.

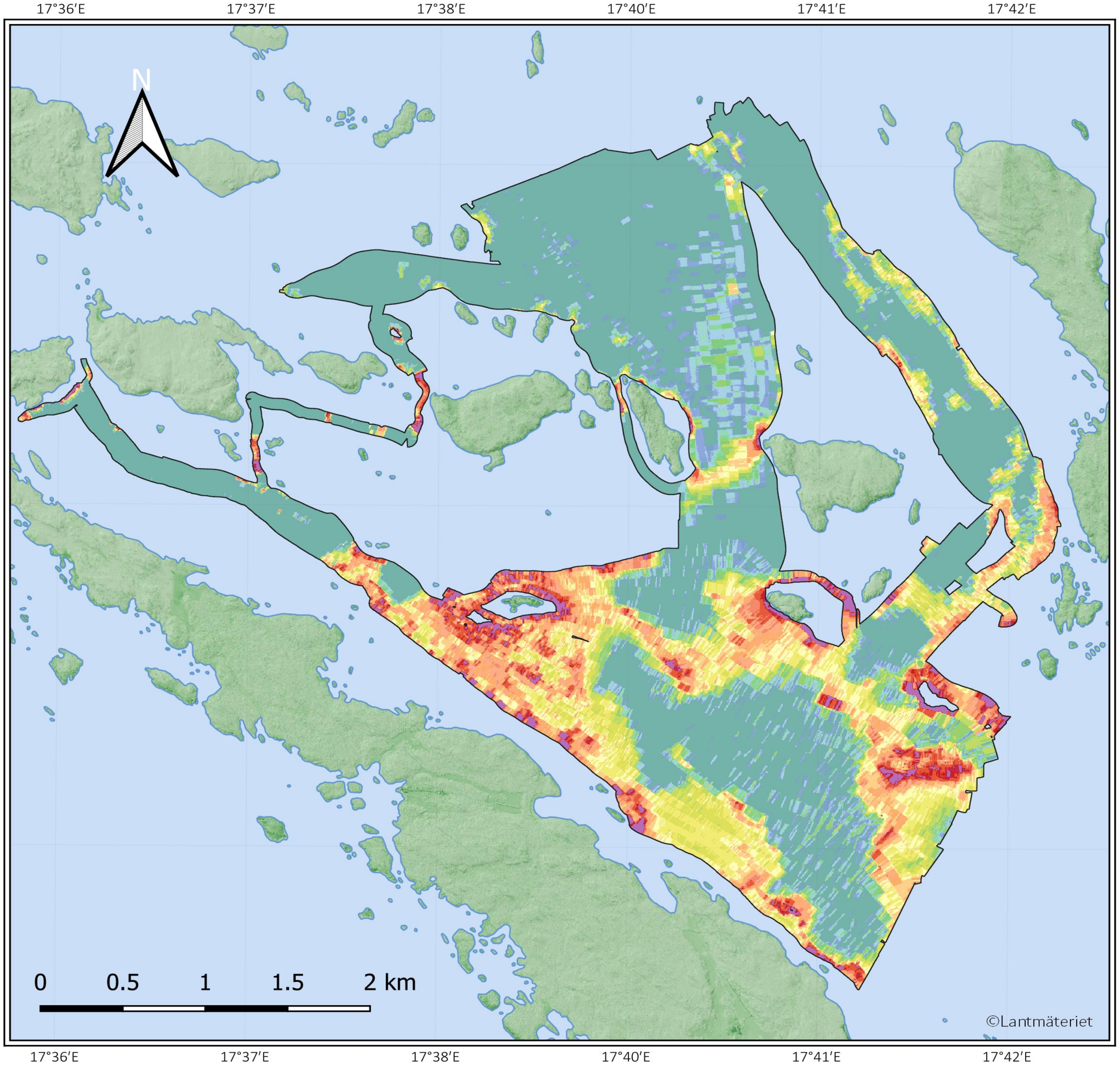

Bottom Habitat Map
East of Askö Island

Interpreted Sediments

- clay
- silty clay
- very fine silt
- sandy clay
- fine silt
- sandy mud
- medium silt
- sandy silt
- coarse silt
- clayey sand
- very fine sand
- muddy sand
- silty sand
- fine sand
- medium sand
- medium sand - gravelly muddy sand
- coarse sand - gravelly sand
- coarse sand - sandy gravel
- gravelly coarse sand
- gravel

Map 4. Color-classified seafloor sediments classes based on FMGT generated ARA Characterization. The entire range of twenty sediment classes defined by the processing software are represented in this map. Sediment types are distinguished by different colors and arranged in legend by increasing grain size. Satellite imagery and additional geodata used to create the basemap were provided by Lantmäteriet via the Swedish University of Agricultural Sciences (SLU) geodata portal. Visualizations are projected in Coordinate Reference System (CRS) SWEREF99 18 00, EPSG: 3011.

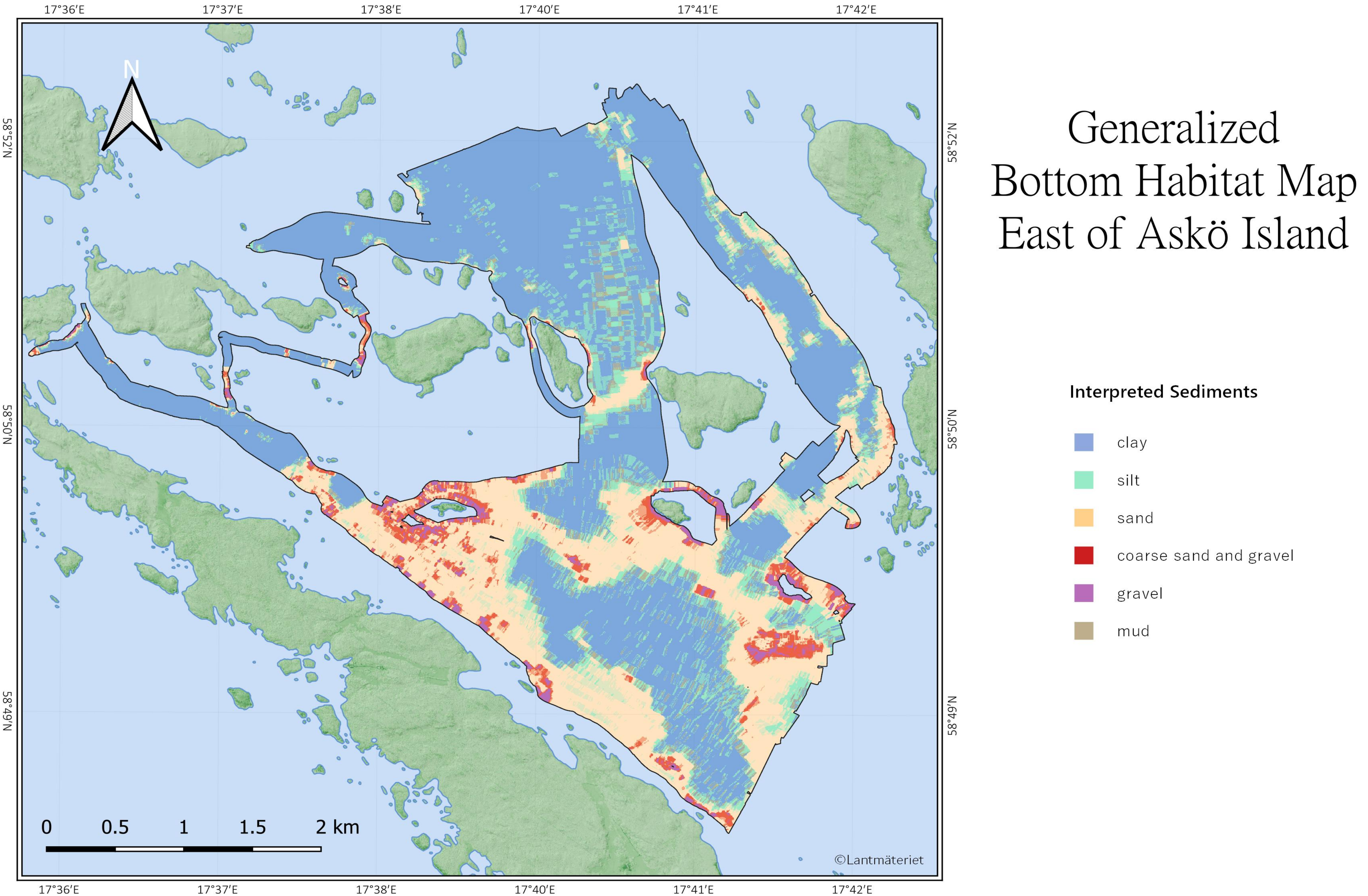

Map 5. Color-classified seafloor sediments classes based on FMGT generated ARA Characterization. Sediment classes are joined based on their primary composition. The sediment types are distinguished by different colors and arranged in the legend according to the area covered by each (decreasing). The entire range of twenty sediment classes defined by the processing software are represented in this map. Satellite imagery and additional geodata used to create the basemap were provided by Lantmäteriet via the Swedish University of Agricultural Sciences (SLU) geodata portal. Visualizations are projected in Coordinate Reference System (CRS) SWEREF99 18 00, EPSG: 3011.

6.2 Comparison to Field Observations

6.2.1 Sediment Core Samples

Five sediment cores collected from the Askö region were used in this study to evaluate the accuracy of software-generated sediment characterizations. A map was generated using QGIS, indicating the precise locations from which the cores were extracted (*Figure 16*). Using the ARA/Benthic Habitat Map as a base, the raster data was interrogated at the extraction points to obtain the characterization values calculated for each location (*Figure 17*).

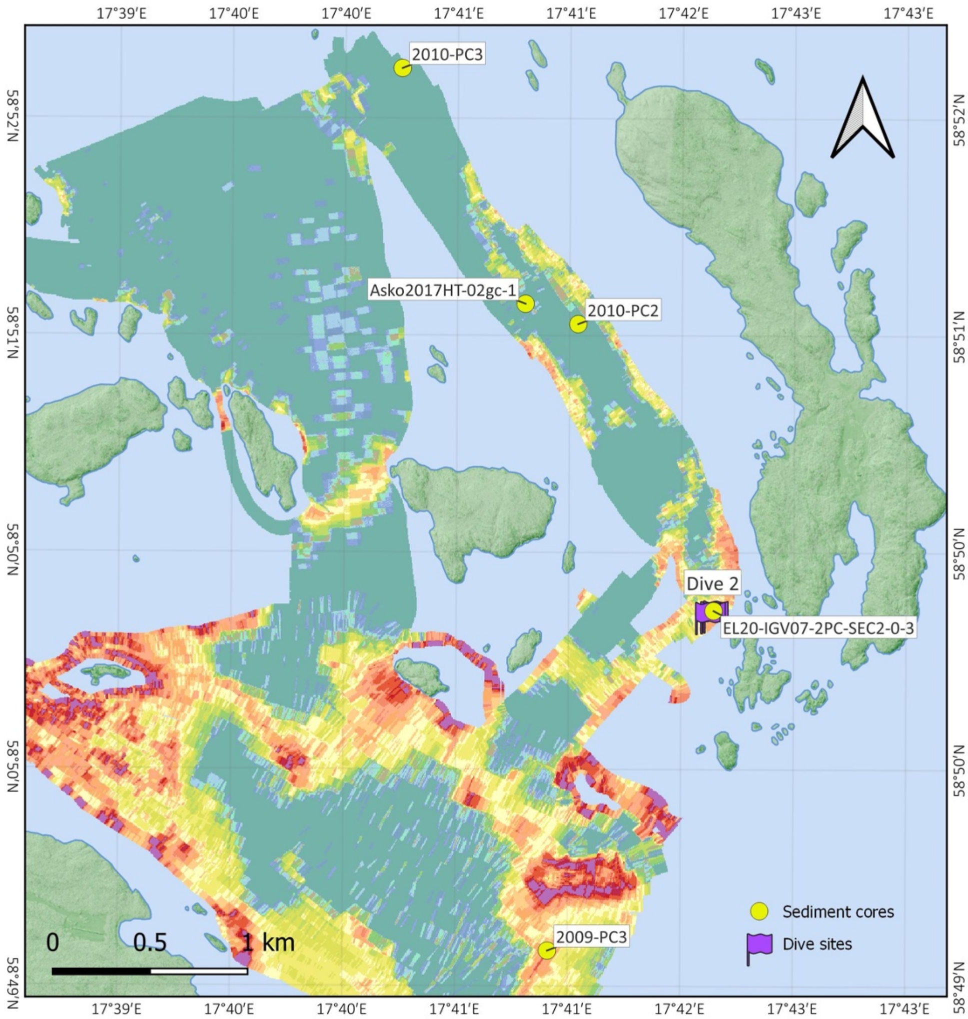

Figure 16. Overview of the location of sediment core extractions and diving investigations relative to the study area. Three closely spaced dive sites and one coring location overlap.

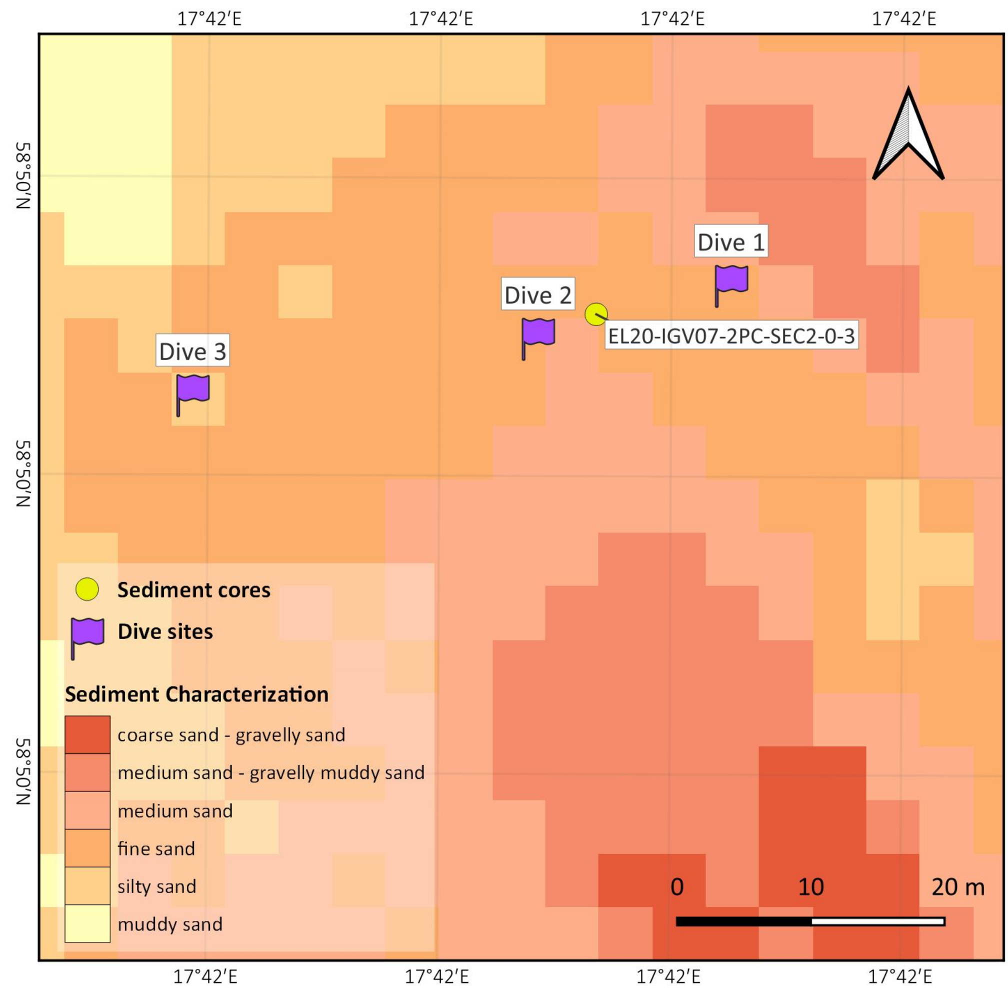

Figure 17. Zoomed view of sediment core and dive sites showing their relationship to the sediment classification of the ARA layer.

The extracted values/classifications were then compared to the descriptions of the sediment samples (*Table 5*). The data presents some disparity between the classifications generated by the software and the ground truth data.

Table 5

Core ID	ARA Characterization		Sediment Core Description
2010-PC2	20	CLAY	mud / ooze
2010-PC3	20	CLAY	muddy clay
2009-PC3	8	SILTY SAND	clay
EL20-IGV07-2PC-SEC2-0-3	7	FINE SAND	clay 75%/v silt 25%/v. Sample vol: 39.9cm3
Asko2017HT-02gc-1	20	CLAY	fine-grained silty clay and gyttja clay Mean: medium silt. Bulk density: 1.34 g/cm3

Table 5. Listed comparison between ARA Characterization values and the sediment interpretations of core samples.

Most of the core descriptions name fine sediments as their primary composition. The ARA likewise reached similar conclusions about the composition of the seafloor. However, it is evident that not all descriptions and generated classifications align.

6.2.2 Underwater Visuals

Three videos of the seafloor were recorded by divers during research investigations in Jakobsson et al., (2020). By relating the still images captured from the videos to their location on the BS mosaic, it is found that the high BS intensity correspond to seabed features. These points were localized on the bathymetry grid to compare the BS signal to the area's terrain (*Figure 18*).

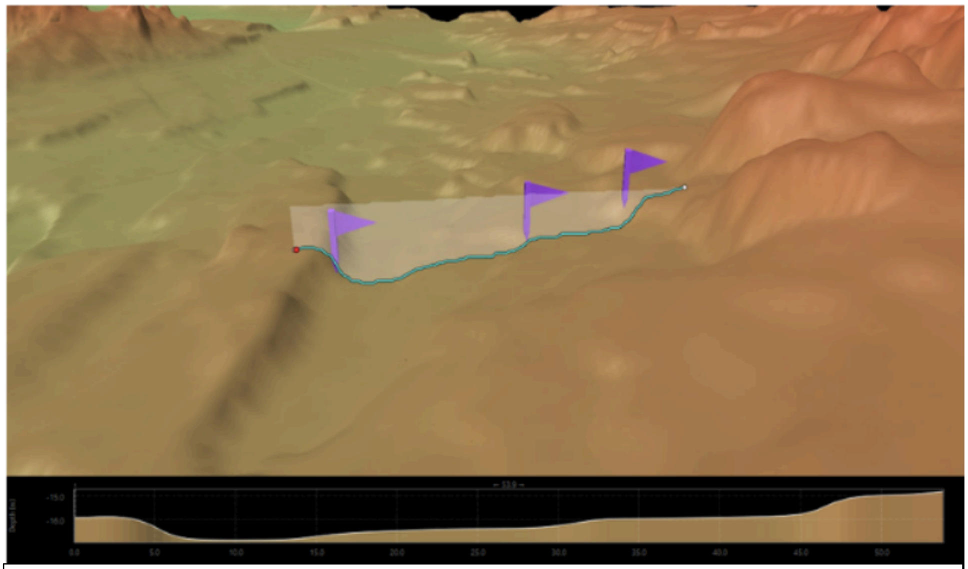

Figure 18. Screen-captured image of the dive sites (represented as purple flags) and their locations on the Qimera bathymetry grid. The seabed's profile along the studied locations is marked by the blue line running across the three flags.

Videos show several "steps", where layered, fine sediments (*Figure 19a*) are capped by a coarser surface. Rocks and pebbles of varied sizes are embedded at the face of the steps as well as scattered along its margins (*Figure 19b*). Communities of mussels atop the surface are also found (*Figure 19c*). The ARA-generated classification defined the sediments at the observed locations as "fine sand" and "silty sand".

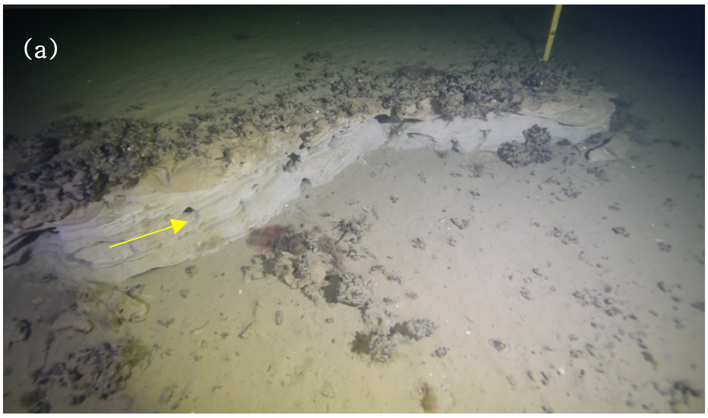

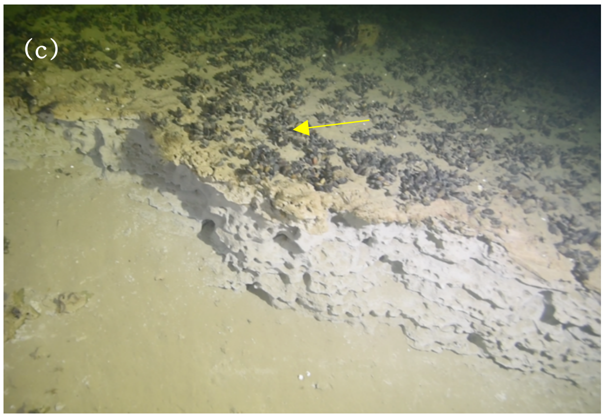

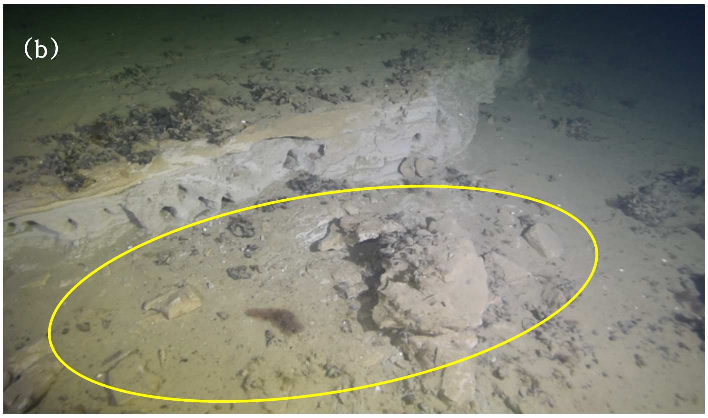

Figure 19. Still images of the videos recorded during dives of the study area. Yellow markings show point at features found: **(a)** Layered sediments **(b)** rocks and pebbles **(c)** mussels on step surface.

6.3 Previous Research on Local Sediments

Previous studies conducted in the area east of Askö define the "steps" seen in the BS mosaic and underwater videos as terraces. These terraces are believed to be formed by groundwater seepage through layers of silty, glacial varved clays (Jakobsson et al., 2020). The terraces are found along the southwestern margins of Fifång (1) and northeastern shore of Askö (2) (Figure 20). Circular depressions defined as pockmarks formed by gas seepage (Jakobsson et al., 2020), appear in the area surrounding the Askö terraces (4). The sediments in the study area are described as primarily formed of Quaternary clay-rich sediments with variations in clay and silt content (Jakobsson et al., 2020).

Figure 20. Landforms found on the seafloor, marked on BS mosaic. 1 indicates the region where terraces are found west of Fifång, and 2, those northeast of Askö. 3 Marks were pockmarks or gas seeps are found.

7. DISCUSSION

7.1 Interpretation of Results

The initial visualization of backscatter data is largely an automatic process on FMGT. Nevertheless, numerous manual adjustments were necessary to reduce artefacts and make the mosaic functional. The resulting representation of the sampled seafloor provided valuable information concerning the characteristics of the study area.

By incorporating the backscatter mosaic into the map of the surrounding islands, the relationship between the backscatter values and surrounding topography can be better appreciated. Seafloor areas immediately bordering Askö reflect stronger backscatter levels. A possible explanation could be that these seafloor areas adjacent to the islands are a continuation of sloping island shores. This would help explain the gradual decrease of backscatter levels (or fining of sediments) as the depth of the seafloor increases. Also, assumed wave activity along shorelines could further rationalize the high backscatter values, as being coarse sediments along the coasts. In thin channels between small, closely neighboring islands, high backscatter intensity values are similarly found.

Inversely, darker areas of low backscatter intensity better relate to the bathymetry of the region. The lowest backscatter levels are found at the deepest areas and expand northward where the seafloor continues uninterrupted by islands. These deep areas, such as Fifångsdjupet could serve as small, sheltered basins allowing the deposition and likely accumulation of finer sediments.

In areas where terraces are found, such as the western margin of Fifång, the presence of large clasts along terrace edges could explain the high backscatter values observed in the BS mosaic. The communities of mussels atop the surface of the terraces could also be represented in the high backscatter signature.

In the ARA interpretations, some misclassifications can be rationalized, for example, those made for 2010-PC3 and 2010-PC2. The ARA characterization scale does not include ooze or muddy clay as sediment classes, possibly resulting in some of these regions being defined by the finest available value – clay. Other incongruencies are not as easily resolved, for example, the classification of clay and silt samples as sand. These could be caused by residual artifacts in the backscatter mosaic.

7.2 Errors and Limitations

Data Collection

Although system calibrations and SVP corrections are routinely performed at the start of every survey, the wide temporal range of the data acquisition process raises the potential for inconsistencies in the data. Additionally, the data used was collected by two different vessels. This could likewise increase the probability of differences due to instrument arrangement and configuration and dissimilarities between the vessels. While processing software attempts to correct for these variables, it is difficult to adequately establish processing parameters for data collected by different vessels, on different occasions, but by the same instrument. There is also the possibility that between the time the surveys were collected, underwater currents, waves, trawling or other human disturbances could have caused changes in distribution of seafloor sediments, possibly masking as interpreted errors.

Data Processing

Data processing on FMGT is a long and sensitive process. Seemingly small changes often require reprocessing the data and rebuilding of the mosaics. Due to the high resolution and large dataset, processing typically took hours after each adjustment. This initial period of data processing consisted mainly of “trial-and-error”, trying to find solutions for inconsistencies. Manual adjustments were made to the backscatter mosaic in areas where specific survey line values did not match the immediately neighboring projections. The adjustments were made with the intention to visually match the values. By doing this, the modified survey lines no longer represent the values directly sampled from the seafloor. Human bias in the backscatter manipulation likely influenced the subsequent layers made during processing. Time restrictions and limited knowledge of the software’s full capabilities resulted in some artefacts remaining in the final backscatter mosaic. These artifacts are clearly be seen in the Statistics map. There is visible striping along survey lines, particularly in areas where curved and straight survey lines overlap. In the ARA map, pixelated “boxing” along some survey lines created patchy areas in otherwise homogenous seafloor sections. The same pattern is seen in the Benthic Habitat Map, where the boxy patches are characterized as lines of silt surrounded by clay. Since no in-situ investigations were made in these regions, it remains unclear if these are accurate sediment representations or artefacts due to processing errors, although the latter is highly probable.

Ground Truths

This project used sediment core sample data from student reports where specific landforms were studied. Due to this reason, the available samples were minimal and covered only a portion of the surveyed seafloor. In addition, the cores were described by general sediment class, but did not incorporate quantifiable grain size values.

In FMGT, ARA characterization can be manually adjusted based on known sediment grain size. It is then possible to apply corrections to the entire layer. However, due to the limited ground truth data available, such comparisons were not possible. In theory, an ARA layer could have been created based on observed sediments and compared for accuracy with one generated using only backscatter data.

The correlation between the "true" sediments and generated classifications relied on the descriptions of the few sampled locations. Considering these limitations, the Bottom Habitat Map is a broad generalization or "segmentation", and the accuracy of the sediment classification cannot be corroborated throughout the entire survey area.

7.4 Recommendations for Future Studies

Ideally, surveys aimed at the interpretation of seafloor sediments based on backscatter should be conducted on a single occasion or closely spaced intervals, utilizing the same vessel and systems. However, in the many cases when this might not be possible, obtaining comprehensive ground truth data becomes crucial for the interpretation of acoustic data. The number of collected sediment samples should reflect the extent of the area being studied. Also, consistent descriptors of grain size during in-situ investigations would greatly simplify postprocessing adjustments.

When time and resources permit, conducting interdisciplinary seafloor surveys can facilitate the interpretation of seafloor composition. For instance, incorporating observations about the benthic fauna/ communities of a region can support sediment classifications based on species preferences or needs.

The recent surge in seafloor mapping and exploration has highlighted the need to optimizing available survey systems and processing software. Steady improvements are continually made, and proprietary algorithms are closely guarded. In future studies, programming knowledge would be greatly beneficial for manipulating the data and products generated by different software platforms.

8. CONCLUSION

The findings in this study show that seabed sediment classifications cannot be made with certainty based solely on acoustic backscatter data. While this data is useful in providing a general representation of the seafloor's composition, it is not entirely accurate. Without the use of substantial ground-truthing data, the sediment characterization made by software algorithms cannot be adequately verified.

Previous research concerning the sediments in the study region show that the general interpretation of the seafloor as "clay" based on backscatter, is correct. The backscatter data also demonstrates a strong correlation to the measured intensities and the geomorphology of the study area seen at the explored dive sites.

9. REFERENCES

Beckholmen, M. and Tirén, S.A., 2008, The geological history of the Baltic Sea a review of the literature and investigation tools, September 2008: Swedish Ratiation Safety Authority, Report2009:21, https://www.stralsakerhetsmyndigheten.se/contentassets/57cf57d0c5f24e3996e97ef1a819cad8/200921-the-geological-history-of-the-baltic-sea-a-review-of-the-literature-and-investigation-tools.

Brown, C.J., Smith, S.J., Lawton, P., and Anderson, J.T., 2011, Benthic habitat mapping: A review of progress towards improved understanding of the spatial ecology of the seafloor using acoustic techniques: Estuarine, Coastal and Shelf Science, v. 92, p. 502–520, doi:10.1016/j.ecss.2011.02.007.

Che Hasan, R., Ierodiaconou, D., Laurenson, L., and Schimel, A., 2014, Integrating Multibeam Backscatter Angular Response, Mosaic and Bathymetry Data for Benthic Habitat Mapping (S. Thrush, Ed.): PloS ONE, v. 9, p. e97339, doi:10.1371/journal.pone.0097339.

Diaz, R.J., Solan, M., and Valente, R.M., 2004, A review of approaches for classifying benthic habitats and evaluating habitat quality: Journal of Environmental Management, v. 73, p. 165–181, doi:10.1016/j.jenvman.2004.06.004.

Engqvist, A., and Andrejev, O., 2003, Water exchange of the Stockholm archipelago—a cascade framework modelling approach: Journal of Sea Research, v. 49, p. 275–294, doi:10.1016/s1385-1101(03)00023-6.

Folk, R.L., Andrews, P.B., and Lewis, D.W., 1970, Detrital sedimentary rock classification and nomenclature for use in New Zealand: New Zealand Journal of Geology and Geophysics, v. 13, p. 937–968, doi:10.1080/00288306.1970.10418211.

Fonseca, L., Brown, C., Calder, B., Mayer, L., and Rzhanov, Y., 2009, Angular range analysis of acoustic themes from Stanton Banks Ireland: A link between visual interpretation and multibeam echosounder angular signatures: Applied Acoustics, v. 70, p. 1298–1304, doi:10.1016/j.apacoust.2008.09.008.

Fonseca, L., and Calder, B., 2009, Geocoder: An efficient Backscatter map constructor in Proceedings, U.S. Hydrographic Conference, Center for Coastal and Ocean Mapping, San Diego, March 2005: Hydrographic Society of America, http://ushydro.thsoa.org/hy05/08_3.pdf.

Fonseca, L., and Mayer, L., 2007, Remote estimation of surficial seafloor properties through the application Angular Range Analysis to multibeam sonar data: Marine Geophysical Research, v. 28, p. 119–126, doi:10.1007/s11001-007-9019-4.

GEBCO Compilation Group (2022) GEBCO 2022 Grid (doi:10.5285/e0f0bb80-ab44-2739-e053-6c86abc0289c)

Head, M.J., Seidenkrantz, M.-S., Janczyk-Kopikowa, Z., Marks, L., and Gibbard, P.L., 2005, Last Interglacial (Eemian) hydrographic conditions in the southeastern Baltic Sea, NE Europe, based on dinoflagellate cysts: Quaternary International, v. 130, p. 3–30, doi:10.1016/j.quaint.2004.04.027.

Hill, C., and Wallström, K., 2008. The Stockholm Archipelago. In: Schiewer, U. (eds) Ecology of Baltic Coastal Waters. Ecological Studies, v. 197, p. 309-334. Springer, Berlin, Heidelberg. doi:10.1007/978-3-540-73524-3_14.

International Hydrographic Organization, IHO (2005). Manual on Hydrography 1th Edition, Publication C-13, 1th Edition, Cha.1, p.14, Cha.3, p.186 2005. Monaco: International Hydrographic Bureau.

Jakobsson, M., Björck, S., Alm, G., Andrén, T., Lindeberg, G., and Svensson, N.-O., 2007, Reconstructing the Younger Dryas ice dammed lake in the Baltic Basin: Bathymetry, area and volume: Global and Planetary Change, v. 57, p. 355–370, doi:10.1016/j.gloplacha.2007.01.006.

Jakobsson, M., Gyllencreutz, R., Mayer, L.A., Dowdeswell, J.A., Canals, M., Todd, B.J., Dowdeswell, E.K., Hogan, K.A., and Larter, R.D., 2016, Mapping submarine glacial landforms using acoustic methods: Geological Society, London, Memoirs, v. 46, p. 17–40, doi:10.1144/m46.182.

Jakobsson, M., Stranne, C., O'Regan, M., Greenwood, S.L., Gustafsson, B., Humborg, C., Weidner, E., 2019. Bathymetric properties of the Baltic Sea. Ocean Science 15(4), 905-916. doi: 10.5194/os-15-905-2019.

Jakobsson, M., O'Regan, M., Mörth, C.-M., Stranne, C., Weidner, E., Hansson, J., Gyllencreutz, R., Humborg, C., Elfwing, T., Norkko, A., Norkko, J., Nilsson, B., and Sjöström, A.: Potential links between Baltic Sea submarine terraces and groundwater seeping, Earth Surf. Dynam., 8, 1–15, https://doi.org/10.5194/esurf-8-1-2020.

Jönsson, A., Lindström, M., Carman, R., Mörth, C.-M., Meili, M., and Gustafsson, Ö., 2005, Evaluation of the Stockholm Archipelago sediments, northwestern Baltic Sea Proper, as a trap for freshwater runoff organic carbon: Journal of Marine Systems, v. 56, p. 167–178, doi:10.1016/j.jmarsys.2004.11.001.

Kautsky, H., 2008, Askö Area and Himmerfjärden, in Schiewer, U., eds., Ecology of Baltic Coastal Waters: Ecological Studies, Springer, Berlin, Heidelberg, v. 197, p. 335–360, doi:10.1007/978-3-540-73524-3_15.

Kenny, A.J., Cato, I., Desprez, M., Fader, G., Schüttenhelm, R.T.E., Side, J., 2003. An overview of seabed-mapping technologies in the context of marine habitat classification. ICES Journal of Marine Science 60(2), 411–418. doi: 10.1016/S1054-3139(03)00006-7.

Kostylev, V. E., Todd, B. J., Fader, G. B. J., Courtney, R. C., Cameron, G. D. M., & Pickrill, R. A., 2001, Benthic habitat mapping on the Scotian Shelf based on multibeam bathymetry, surficial geology and sea floor photographs. Marine Ecology Progress Series, 219, 121–137. http://www.jstor.org/stable/24864820

Lamarche, G., Lurton, X., Verdier, A.-L., and Augustin, J.-M., 2011, Quantitative characterisation of seafloor substrate and bedforms using advanced processing of multibeam backscatter—Application to Cook Strait, New Zealand: Continental Shelf Research, v. 31, p. S93–S109, doi:10.1016/j.csr.2010.06.001.

Leppäranta, M., and Myrberg, K., 2009, Physical Oceanography of the Baltic Sea: Springer Berlin Heidelberg, doi:10.1007/978-3-540-79703-6.

Lurton, X., 2010, Underwater acoustic wave propagation in An introduction to underwater acoustics: Principles and applications (second edition): Berlin, Germany, Springer, p.15-74.

Lurton, X., Lamarche, G., Brown, C., Lucieer, V., Rice, G., Schimel, A., and Weber, T., 2015, Backscatter measurements by seafloor-mapping sonars: guidelines and recommendations:, https://hdl.handle.net/102.100.100/23072081.v1

Mackenzie, K.V., 1981, Nine-term equation for sound speed in the oceans: The Journal of the Acoustical Society of America, v. 70, p. 807–812, doi:10.1121/1.386920.

Parnum, I.M., and Gavrilov, A.N., 2011, High-frequency multibeam echo-sounder measurements of seafloor backscatter in shallow water: Part 2 – Mosaic production, analysis and classification: Underwater Technology, v. 30, p. 13–26, doi:10.3723/ut.30.013.

Schiewer, U., 2008. Introduction, in Schiewer, U. (eds) Ecology of Baltic Coastal Waters: Ecological Studies, v. 197, p. 1-22. Springer, Berlin, Heidelberg. doi:10.1007/978-3-540-73524-3_1.

Shepard, F.P., 1954, Nomenclature Based on Sand-silt-clay Ratios: SEPM Journal of Sedimentary Research, v. Vol. 24, doi:10.1306/d4269774-2b26-11d7-8648000102c1865d.

Šliaupa, S., and Hoth, P., 2011, Geological Evolution and Resources of the Baltic Sea Area from the Precambrian to the Quaternary, in Harff, J., Björck, S., and Hoth, P. (Eds.), The Baltic Sea Basin: Springer Berlin Heidelberg, p. 13–51, doi:10.1007/978-3-642-17220-5_2.

Smith, J., O'Brien, P.E., Stark, J.S., Johnstone, G.J., and Riddle, M.J., 2015, Integrating multibeam sonar and underwater video data to map benthic habitats in an East Antarctic nearshore environment: Estuarine, Coastal and Shelf Science, v. 164, p. 520–536, doi:10.1016/j.ecss.2015.07.036.

Swärd, H., O'Regan, M., Ampel, L., Ananyev, R., Chernykh, D., Flodén, T., Greenwood, S.L., Kylander, M.E., Mörth, C.M., Preto, P., and Jakobsson, M., 2015. Regional deglaciation and postglacial lake development as reflected in a 74 m sedimentary record from Lake Vättern, southern Sweden: GFF, v. 138, p. 336–354, doi:10.1080/11035897.2015.1055510.

Tuuling, I., Bauert, H., Willman, S., & Budd, G., 2011, The Baltic Sea : Geology and geotourism highlights. Retrieved from http://urn.kb.se/resolve?urn=urn:nbn:se:uu:diva-165058

Walton, K., García-García, A., and Endris, C., 2016, Potential marine benthic habitat map of Elkhorn Slough, California: Regional Studies in Marine Science, v. 8, p. 210–215, doi:10.1016/j.rsma.2016.08.007.

White, J., Jegat, V., Van Lancker, V., Deleu, S., and Vanstaen, K., 2007, Multibeam echo sounders in Coggan, R., Populus, J., White, J, Sheehan, K., Fitzpatrick, F. and Piel, S. eds., 2007 Review of Standards and Protocols for Seabed Habitat Mapping. MESH, 53-70 p.

Wiklund, A.-K.E., Malm, T., Honkakangas, J., and Eklund, B., 2012, Spring development of hydrolittoral rock shore communities on wave-exposed and sheltered sites in the northern Baltic proper: Oceanologia, v. 54, p. 75–107, doi:10.5697/oc.54-1.075.

Winterhalter, B., Flodén, T., Ignatius, H., Axberg, S., and Niemistö, L., 1981, Geology of the Baltic Sea, in The Baltic Sea: Elsevier Oceanography Series v. 30, p. 1–121, doi:10.1016/s0422-9894(08)70138-7.